universität wien

MASTERARBEIT / MASTER'S THESIS

Titel der Masterarbeit / Title of the Master's Thesis

„Molecular and morphological mechanisms in the ovary of middle-aged mice causing delayed Progesterone withdrawal“

verfasst von / submitted by

Severin Bachmayer, BSc

angestrebter akademischer Grad / in partial fulfilment of the requirements for the degree of

Master of Science (MSc)

Wien, 2024 / Vienna 2024

Studienkennzahl lt. Studienblatt / degree programme code as it appears on the student record sheet:	UA 066 220
Studienrichtung lt. Studienblatt / degree programme as it appears on the student record sheet:	Joint-Masterstudium Evolutionary Systems Biology UG2002
Betreut von / Supervisor:	Univ.-Prof. Mag. Dr. Mihaela Pavličev
Mitbetreut von / Co-Supervisor:	

Table of contents

1 Abstract

In most mammals, reproductive function declines or ceases before the end of their life span. Albeit reproductive aging is a well-appreciated phenomenon, its underlying mechanisms are poorly understood. The present work focuses on reproductive aging mechanisms in mice. Early aging complications in reproduction of female mice have been reported to affect late pregnancy and parturition. Thereby, systemic progesterone withdrawal, which is normally caused by luteolysis to trigger parturition, is delayed in older mice. Thus, we hypothesize that the cause for age-related dystocia is likely connected to a defect in luteolysis. Here, we investigate the morphological and molecular mechanisms of PGF2α-induced luteolysis in late murine pregnancy using histology, steroid hormone assays and transcriptome analysis. We show that in our C57BL/6 mouse line, the corpus luteum of late pregnancy is characterized by autophagosome formation, and that luteolysis has not occurred at 17.5 days post conception. Comparing ovarian morphology of late pregnant 8-month old and 3-month old mice, we find age-related accumulations of enlarged, hemosiderin-laden macrophages. These are considered to be markers of chronic inflammation. In the Corpus luteum, we also find an age-related expression increase of inflammatory marker genes, and an expression decrease of genes related to mitosis checkpoint signaling and DNA replication, which are potential signs of DNA damage. We propose that the 8-month old murine ovary is characterized by inflammaging, which may lead to dysregulation of Progesterone activity due to its own anti-inflammatory properties.

1 Zusammenfassung

Bei den meisten Säugetieren nimmt die Fortpflanzungsfähigkeit vor dem Ende der Lebensspanne ab oder sistiert. Obwohl das Phänomen des reproduktiven Alterns gut bekannt ist, sind die zugrundeliegenden Mechanismen nur begrenzt geklärt. Die vorliegende Arbeit konzentriert sich auf die Mechanismen des reproduktiven Alterns bei Mäusen. Berichten zufolge beeinträchtigen frühe Alterskomplikationen bei der Reproduktion weiblicher Mäuse späte Schwangerschaftsstadien und die Geburt. So ist der systemische Progesteronentzug, welcher normalerweise durch die Luteolyse getriggert wird und die Geburt auslöst, bei älteren Mäusen verzögert. Daher stellen wir die Hypothese auf, dass die Ursache für die altersbedingte Dystokie wahrscheinlich mit einem Defekt der Luteolyse zusammenhängt. Im Folgenden untersuchen wir die morphologischen und molekularen Mechanismen der PGF2α-induzierten Luteolyse in späten Schwangerschaftsstadien von Mäusen mithilfe von Histologie, Steroidhormon-Assays und Transkriptomanalyse. Wir zeigen, dass in unserer C57BL/6-Mauslinie der Corpus luteum der späten Schwangerschaft durch Bildung von Autophagosomen charakterisiert ist, und dass die Luteolyse 17,5 Tage nach der Befruchtung noch nicht begonnen hat. Beim morphologischen Vergleich der Ovarien schwangerer Mäuse im Alter von 8 Monaten und 3 Monaten finden wir altersbedingte Ansammlungen vergrößerter, Hämosiderin enthaltender Makrophagen. Diese gelten als Zeichen chronischer Entzündung. Im Corpus luteum finden wir auch einen altersbedingten Expressionsanstieg von Entzündungsmarkergenen und einen Expressionsrückgang von Genen, die mit der Signalisierung von Mitose-Kontrollpunkten und der DNS-Replikation in Zusammenhang stehen, was auf potenzielle Anzeichen von DNS-Schäden hindeutet. Wir vermuten, dass das 8 Monate alte Ovarium von Mäusen von Entzündungsaltern geprägt ist, was aufgrund der entzündungshemmenden Eigenschaften von Progesteron zu einer Dysregulation der Progesteron-Aktivität führen kann.

2 Introduction

The mystery of why and how we age has fascinated scientists and philosophers for millennia, and physiological aging studies on model organisms date back nearly a century (Cohn & Lange 1930, Baars 2012). With the advent of omics, many molecular hallmarks of the aging process have been elucidated, and the field has seen a renewed surge of interest (López-Otín et al. 2013, 2023, Kennedy et al. 2014, Kaeberlein & Tyler 2021). These genomic, proteomic and metabolomic hallmarks are interconnected and mutually reinforcing, and do not necessarily occur systemically, but can occur locally limited within one organism, developing at different speeds in different organs (Horvath et al. 2015, Baechle et al. 2023). Indeed, a multi-omics study recently demonstrated that human organs age at different rates (Nie et al. 2022). Especially when looking at reproductive organs, this appears to hold true for placental mammals in general as female reproductive organs, in particular the ovary, show functional decline at a relatively young age in humans, rodents and ruminants alike (Rubin 2000, Kordowitzki et al. 2021, Camaioni et al. 2022, Sirard 2022, Montenegro et al. 2023). Mice are a key mammalian model organism in aging research, and various studies on reproductive aging in the murine ovary been conducted to date (Asano 2012, Vanhooren & Libert 2013, Isola et al. 2023). These studies report the accumulation of senescence markers, chronic inflammation, accelerated fibrosis and shifts in macrophage populations (Briley et al. 2016, Urzua et al. 2018, Zhang et al. 2020).

Most such investigations use mice near (or even past) the end of their reproductive phase. However, the consequences of reproductive aging are already severe, and often fatal, at a much younger age. Patel et al. (2017) compared pregnancy between 8-month old C57BL/6 mice (akin to a 32 year-old human) and 3-month old mice (akin to a 20 year-old human), and demonstrated that the process of parturition is dysfunctional (Flurkey et al. 2007). In 8-month old (hereafter old) mice, gestation time is increased by 24 hours, the duration of labor is more than doubled, and myometrial contractility is diminished compared to 3-month old mice (hereafter young), leading to dystocia and a 25% mortality rate of both mother and offspring due to unsuccessful delivery. Patel et al. attribute these age-related differences to a delay in systemic Progesterone (hereafter P4) withdrawal. Concurrent with this, previous data from our own group also shows an age-related delay in P4 withdrawal in on C57BL/6 mice, and an increase in dystocia incidence in a cross of two inbred lines, Large and Small (LG x SM, Jackson Labs, Maine; Pavličev unpublished, Fig. 1). While Patel et al. provide a mechanistic description of the effects of delayed P4 withdrawal and show that it is connected to age, the question of how the two are related remains. Thus, we want to elucidate why and how aging impairs P4 withdrawal by taking a closer look at the P4 withdrawal mechanism and upstream signalling pathways in the ovary, and more specifically the Corpus luteum (hereafter CL), the main source of P4 in murine pregnancy.

As one of the first hormones identified as a central player in placental pregnancy, P4 is neatly named for its function as a pro-gestational steroid ketone. Due to its inhibitory effect on inflammatory pathways, P4 keeps inflammation at bay during embryo implantation and decidualization. It is also necessary to maintain the structural integrity of the cervix and myometrial quiescence alike (Larsen & Hwang 2011, Wilson & Mesiano 2020). P4 is produced in the CL, a transient gland that forms from an ovarian

follicle after ovulation, triggered by a luteinizing hormone signal from the anterior pituitary gland. Multiple CL are formed per cycle, and if embryo implantation occurs, they persist throughout pregnancy, maintaining it by producing and secreting P4 (Stocco et al. 2007). At the end of pregnancy (or in absence of implantation), the endometrium starts to synthesize Prostaglandin F2α (hereafter PGF2α), which is then transported to the ovary by blood. In the CL, it binds to its receptor PTGFR to initiate the partially redundant, multi-pathway PGF2α signaling cascade (Sugimoto et al. 1998). PGF2α signaling induces the structural and functional degradation of the CL, or luteolysis (McCracken et al. 1999, Davis and Rueda 2002). PGF2α signaling causes luteolysis by inhibition of P4 synthesis, catabolism of P4, and induction of apoptotic and autophagic cell death of the P4-producing Granulosa Lutein Cells (hereafter GLCs) and Theca Lutein Cells (hereafter TLCs) (Hansel & Convey 1983, Auletta & Flint 1988, Sugino & Okuda 2007, Stocco et al. 2007). The CL regresses, P4 production ceases quickly and systemic P4 levels drop. In the uterus, the withdrawal of P4 initiates parturition by leading to ripening of the previously closed cervix, allowing it to open, and increasing myometrial contractility via induction of oxytocin receptor (Oxtr) and Connexin 43 (Cx43) expression (Lye et al. 1993; Ou et al. 1997; Ou et al. 1998, Larsen & Hwang 2011). As a consequence, the myometrium begins to contract and the offspring is delivered.

Since P4 withdrawal is delayed in old mice, the cause for this age-related dysfunction must lie upstream, in PGF2α - mediated luteolysis. Oddly, previous measurements from our group indicate that endometrial PGF2α production is not reduced, but on the contrary, may even be increased, in old mice (Fig. 1). Thus, it is reasonable to assume that either some aspect of PGF2α signaling, or its effector processes in luteolysis, is defective as a result of aging processes. The induction of luteolysis occurs shortly before parturition; our previous observations suggest that the critical time lies between 15.5 and 17.5 days post conception (hereafter dpc). In this study, we focus on morphological and transcriptomic changes in the young and old mouse ovary of late pregnancy. We show that luteolysis has not yet occurred at 17.5 dpc in our line, and find signs of age-related chronic inflammation in the 8-month old murine ovary.

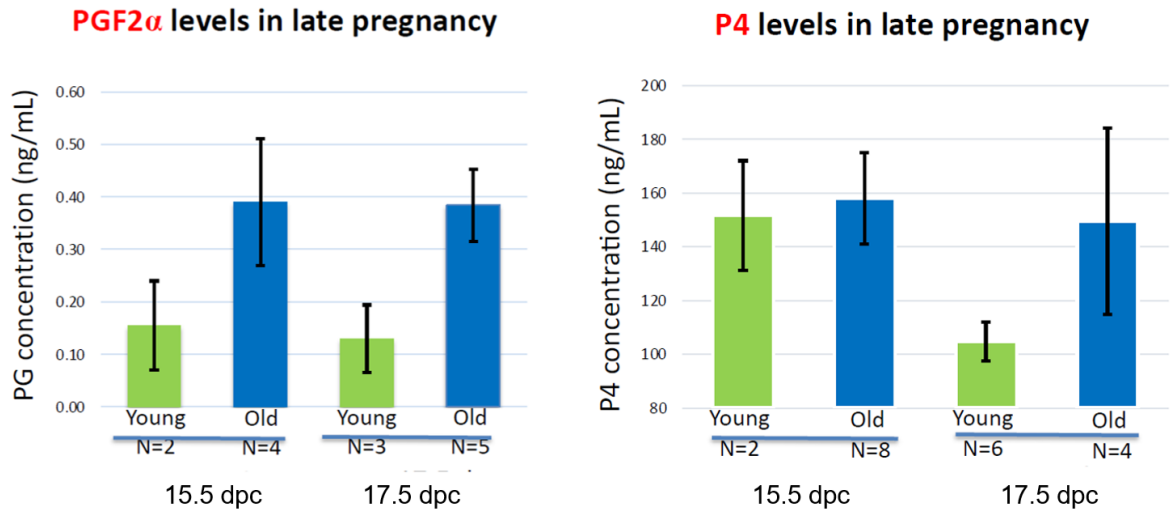

Figure 1. Hormone level measurements of Uterine PGF2α (left) and Serum P4 (right) in young (3-month old) and old (8-month old) mice. Previous data from the Pavličev lab

(unpublished). dpc = days post conception.

3 Materials and Methods

We took a detailed look at the ovary of late pregnancy between 15.5 dpc and 17.5 dpc in young and old C57BL/6 mice. To validate the presence of PGF2α in the ovary as well as the age differences in systemic P4, we measured PGF2α in ovarian tissue and P4 in blood serum by enzyme-linked immunosorbent assay (ELISA). Furthermore, we performed transcriptome analysis to elucidate molecular processes in late pregnant pre-parturition corpora lutea and look for age-related differences with an emphasis on activity of PGF2α signaling and luteolysis components as well as processes related to aging. Finally, we investigated the histological characteristics of structural luteolysis progression at 17.5 dpc via H&E stain and compared ovarian morphology between old and young mice, particularly checking for signs of fibrosis, a hallmark of ovarian aging in mouse. Additionally, we employed Perls' stain to check for age-related increase of senescence markers and macrophages in ovarian tissue.

3.1 Animal husbandry, mating and tissue collection

C57BL/6 mice were kept under controlled conditions at a constant temperature of 21°C and a 12h/12h light/dark cycle in the animal facility of the University Biology Building, according to the approved animal protocol. Animals had access to standard chow and water ad libitum and were kept in groups of a maximum of four individuals of the same sex per cage. Old mice had had one prior litter to confirm reproductive potential. Ovarian cycles were determined by vaginal swab (Byers et al. 2012). When in estrus stage, female mice were paired with male mice overnight and successful copulation was detected by the presence of a copulatory plug on the following morning. In case of the plug, the length of gestation was counted from the midnight of the night preceding the detection of the plug. Both young and old female mice were euthanized for tissue and blood harvesting at 15.5 and 17.5 days post conception (dpc), using cervical dislocation. The four different conditions to be compared were thus: 3-month old at 15.5 dpc (hereafter Y15.5), 3-month old at 17.5 dpc (Y17.5), 8-month old at 15.5 dpc (O15.5) and 8-month old at 17.5 dpc (O17.5). From each mouse, ovaries, kidney and blood were collected. Blood was allowed to clot at RT (21°C) for 30 minutes, then spun down at 1.700 x g for 20 minutes to isolate serum, which was stored at -70°C until further use. One of the ovaries was cut in half. One half was flash frozen in liquid nitrogen, then stored at -70°C until further use. The other half was used for histology. The other ovary was transferred to a petri dish with RNAlater (Ambion®) immediately after collection to prevent RNA degradation. Corpora lutea were isolated from this ovary by microdissection, then stored in fresh RNAlater at -20°C.

3.2 Progesterone and Prostaglandin F2α assays

Progesterone concentration in blood serum was measured in triplicate by competitive ELISA using a Mouse Progesterone ELISA kit (ChrystalChem®) according to the manufacturer's instructions. Flash frozen ovarian tissue samples were weighed and homogenized in 70% EtOH. Then, EtOH was evaporated under N2 before re-suspending samples in extraction buffer from the commercial Mouse PGF2α ELISA kit used to perform competitive ELISA. The plate was washed, then 50µl of sample and

50µl of Biotin-labeled PGF2α antibody were added to the well in duplicate, mixed thoroughly and incubated at 37°C for 45 minutes. Then, the solution was aspirated and the plate washed before adding 100 µl Streptavidin-HRP conjugate solution and incubating at 37°C for 30 minutes. After subsequent aspiration and washing, 90 µl TMB substrate solution was added and incubated at 37°C. After 10 and 15 minutes, colour intensity was checked and 50µl stop solution added. PGF2α concentration was assessed by measuring optical density, and normalizing in each sample by the amount of tissue entering the analysis, using a microplate reader (Spectramax ABS Plus, Molecular Devices®) and the SoftMax Pro software (Version 7.1, Molecular Devices®).

3.3 RNA extraction and purification

To extract mRNA from the corpora lutea we used an RNeasy Micro Kit (Qiagen®), suspending the tissue in the provided extraction buffer before homogenizing it for 50 seconds using a tissue homogenizer (Precellys Evolution, Avantor®). Then, potential contamination with DNA was removed using a TURBO DNA-free® kit (Ambion®) and purified RNA sent to Novogene® for 150 bp paired-end Illumina sequencing.

3.4 Differential gene expression analysis and GO enrichment analysis

Quality control of the obtained raw paired-end Illumina reads was done using the FastQC sequence quality control tool (Andrews 2010). Then, reads were mapped to the mouse genome using STAR (Dobin et al. 2013). The mapped reads were imported into R for analysis. All genes with read count ≥ 10 were considered expressed, the rest were excluded from downstream analysis. Unsupervised sample clustering analysis was done by calculating Spearman's ρ and visualizing correlations via heatmap to compare global expression profiles and identify potential outliers. After applying variance stabilizing transformation, principal component analysis was performed to explore whether age and dpc are the major sources of between-sample variation. Then, differential gene expression (DGE) analysis was done using R package DESeq2 (Love et al. 2014). The DESeq2 standard Median of Ratios method was chosen for normalization (Ander & Huber 2010). This method calculates an individual size factor based on the median ratio of gene counts relative to the geometric mean expression of all samples per gene for each individual gene to account for differences in library size, sequencing depth and RNA composition. Then we performed LFC (Log fold change) shrinkage to account for genes with low counts and high dispersion using R package apeglm (Zhu et al. 2019). Genes were tested for significant differential expression using the Wald test (Wald 1943), before correction for multiple testing by employing the Benjamini-Hochberg method (Benjamini & Hochberg 1995). Samples were first compared pair-wise, then grouped by age and day post conception (15.5 vs 17.5) and cross-compared. Finally, we investigated the molecular and biological function of genes with significant expression change, prioritizing genes that were both differentially expressed and part of the GOI list, mentioned previously. To discover gene sets with a shared biological function that were over- or underrepresented in individual samples we conducted a Gene ontology (GO) enrichment analysis of differentially expressed genes with LFC ≥ 0.5 and ≤ -(0.5), respectively. We used the Panther classification system for unranked GO analysis and GOrilla tool for ranked GO analysis (Mi et al. 2013, Eden et al. 2009).

3.5 Selection of Genes of Interest

The online gene ontology enrichment analysis database QuickGO was browsed for GO terms relating to synthesis, regulation, metabolism and downstream targets of the two main players, PGF2α (and its receptor PTGFR), P4 as well as any term related to the luteolysis process. GO annotations for eleven different GO terms were selected (Tab. 2). Though an emphasis was put on mouse (*Mus musculus*) and rat (*Rattus norvegicus*), any GO annotations from human (*Homo sapiens*), cattle (*Bos taurus*), pig (*Sus scrofa*) and sheep (*Ovis gmelina*) were also included for further investigation. The annotations were then checked for more detailed information on their function and connected publications describing their role in the respective process. Additionally, genes of interest (hereafter GOI) were identified by conducting literature searches on Pubmed, Orcid and GoogleScholar using the search terms “luteolysis”, “luteal regression”, “PGF2α (bio)synthesis”, “PGF2α regulation”, “PTGFR”, “Prostaglandin (bio)synthesis”, “Prostaglandin metabolism”, and various combinations thereof. Finally, the genes previously identified to be involved in these processes by GO enrichment analysis in human, cattle, pig and sheep were combined with the above search terms to check for publications describing their involvement in the same process in mouse and rat.

3.6 Histology

Freshly harvested tissue samples were fixed in 4% PFA overnight, washed in PBS, then dehydrated in increasing concentration of ethanol (30% - 50% - 70%, two changes of 30 minutes each) and stored in 70% ethanol at -20°C. For embedding, samples were further dehydrated (80% - 90% - 95% - 100% ethanol, two changes of 30 minutes each), embedded in paraffin, sectioned at 5 µm thickness with a Leica RM2265 microtome and mounted on microscope slides. For staining, the slides were deparaffinized at 60°C overnight, washed in Xylol twice for 10 minutes to remove leftover paraffin, and rehydrated in decreasing concentrations of ethanol (100% - 95% - 70%, 3 minutes each) to dH2O. Next, they were either stained with water-soluble Hematoxylin & Eosin for general morphological comparison or with Perl's stain to identify iron accumulations. Hematoxylin stains cell nuclei blue, while Eosin stains ECM and cytosol pink, and the combination gives different hues dependent on the eosinophilic or basophilic properties of a given cell. Perl's stain causes ferric iron to form an insoluble blue pigment, allowing for the detection of hemosiderin, while staining other intra- and extracellular structures in different shades of pink.

3.7 Imaging

Slides were imaged with an EVOS M7000 Microscope (Thermo Fisher Scientific®). Brightness and contrast of images was adjusted for better presentation using the EVOS Analysis software.

4 Results

4.1 Luteal gene expression levels are consistent in late pregnancy

After FastQC quality control, over 20 million RNA reads were obtained for each sample (O15.5: 2.12 – 2.55 * 10^7 reads; O17.5: 2.12 – 2.47 * 10^7 reads; Y15.5: 2.12 -2.55 * 10^7 reads; Y17.5: 2.03 – 2.58 * 10^7 reads). Relative content of duplicate reads ranged at 51.2 - 57.3 %, with absolute number of unique reads ranging from 8.5 - 12.2 * 10^6 reads per sample. Sample GC content was consistent at 48 - 49%, read sequence length was uniform at 150bp and minimum mean FastQC quality score across all samples was 34.6. STAR Mapping rate ranged from 90.2 % (1.6 * 10^7 uniquely mapped reads) to 93.1 % (2.4 * 10^7 uniquely mapped reads). Accordingly, read counts mapped, and imported into R for DGE analysis ranged between 16 and 24 Million (Fig. 2).

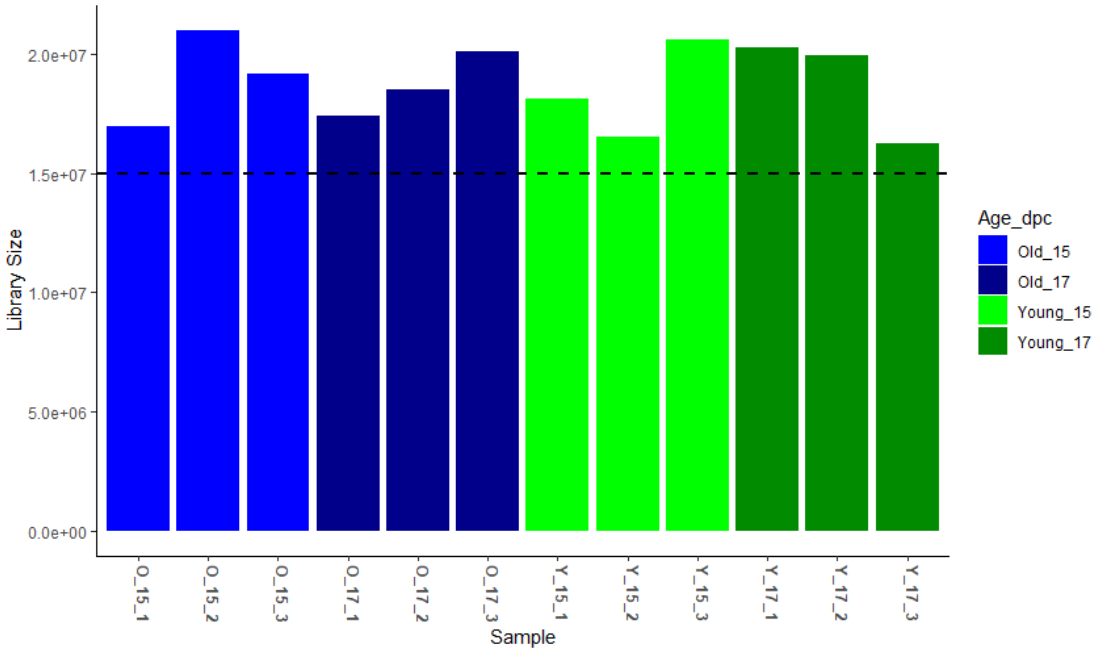

Figure 2. Library sizes of raw read counts. *Dotted line: 15.000.000 counts.*

Number of individual transcripts detected in at least one sample totalled 51312. Of these, 20324 individual transcripts expressed in all replicates of at least one sample group (read count ≥ 10) were included in further analysis. Global gene expression profiles were highly similar among all samples, with Spearman's r > 0.97 between the two least similar ones (Fig. 3). Global expression patterns of the biological replicates did not cluster together better than those between cohorts. One clear outlier appears to be Y17.5_2, and a less apparent outlier is O15.5_1. The rest builds two main clusters, which are separated by age. These also show some inconsistency, as one young (Y17.5_1) groups with the old samples. However, it should be noted that the deviation in clustering is driven by minor differences in otherwise very highly correlated samples.

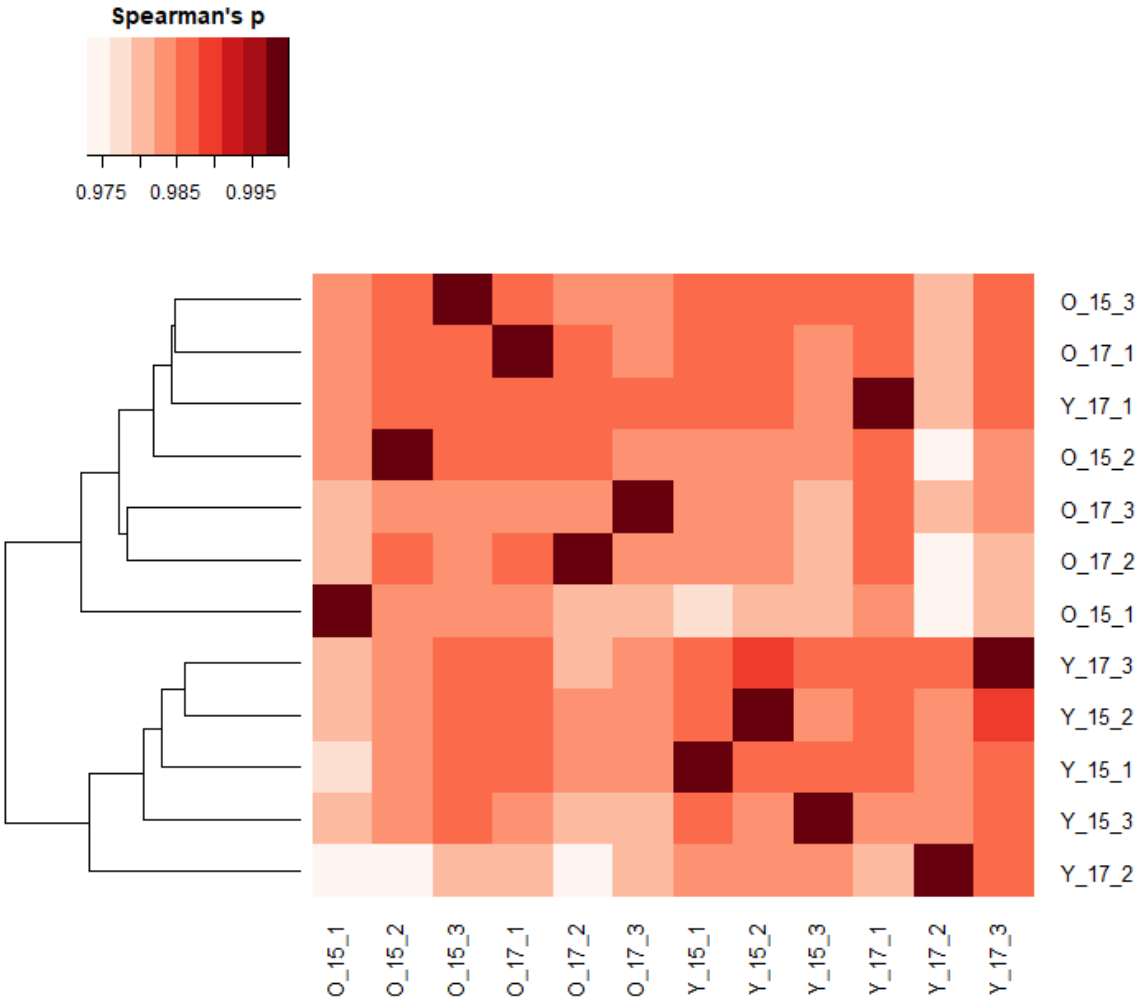

Figure 3. Heatmap of Spearman correlation coefficient between gene expression profiles of the samples.

In PCA, the samples showed clearer grouping: the first principal component differentiates the old and young samples (51% explained variance), although the age groups are not fully separated (Fig. 4A). The separation between 15.5 dpc and 17.5 dpc along PC2 (17.4% explained variance) is clear for old samples, but not for young samples (Fig. 3A). Y17.5_1 appears to cluster with the O17.5 samples rather than with Y17.5_2 and Y17.5_3. Indeed, if Y17.5_1 were omitted, there would be both clear age grouping as well as similar patterns along PC1 and PC2. Still, age appears to be the main driver of PC1. PC2 appears mainly driven by dpc, although this is clearer in old than in young samples. Interestingly, within-sample variance at 15.5 dpc appears to be connected to PC2, while within-sample variance at 17.5 dpc appears to be connected to PC1, suggesting that individual variation is a secondary driver of both PC1 and PC2. There was no clearly distinguishable grouping of samples along PC3 and PC4 (Fig. 4B).

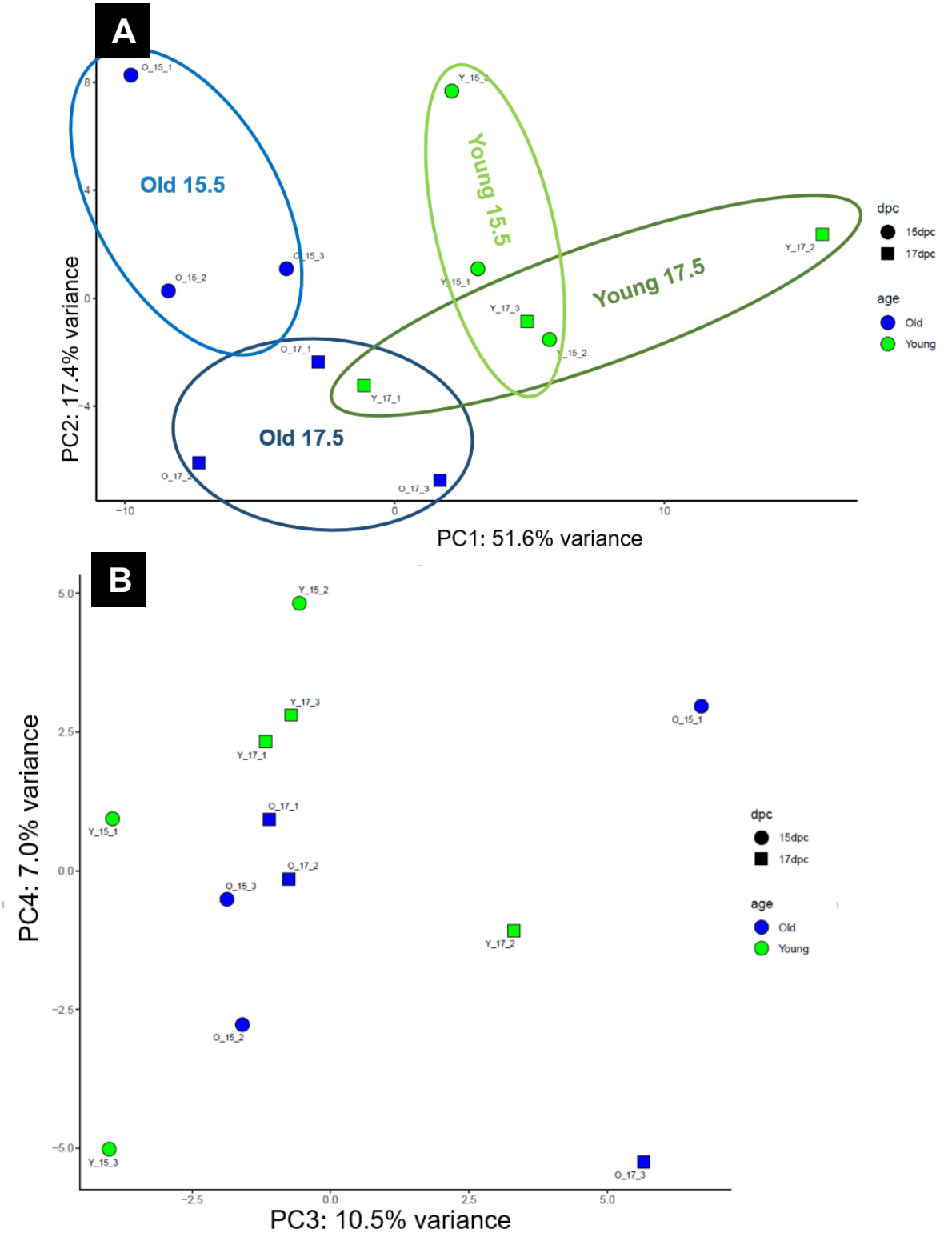

Figure 4. PCA plots. **A** PC1 versus PC2. Samples of different age separate along PC1, while O15.5 and O17.5 separate along PC2. **B** PC3 and PC4 show no recognizable pattern with respect to age and pregnancy progression.

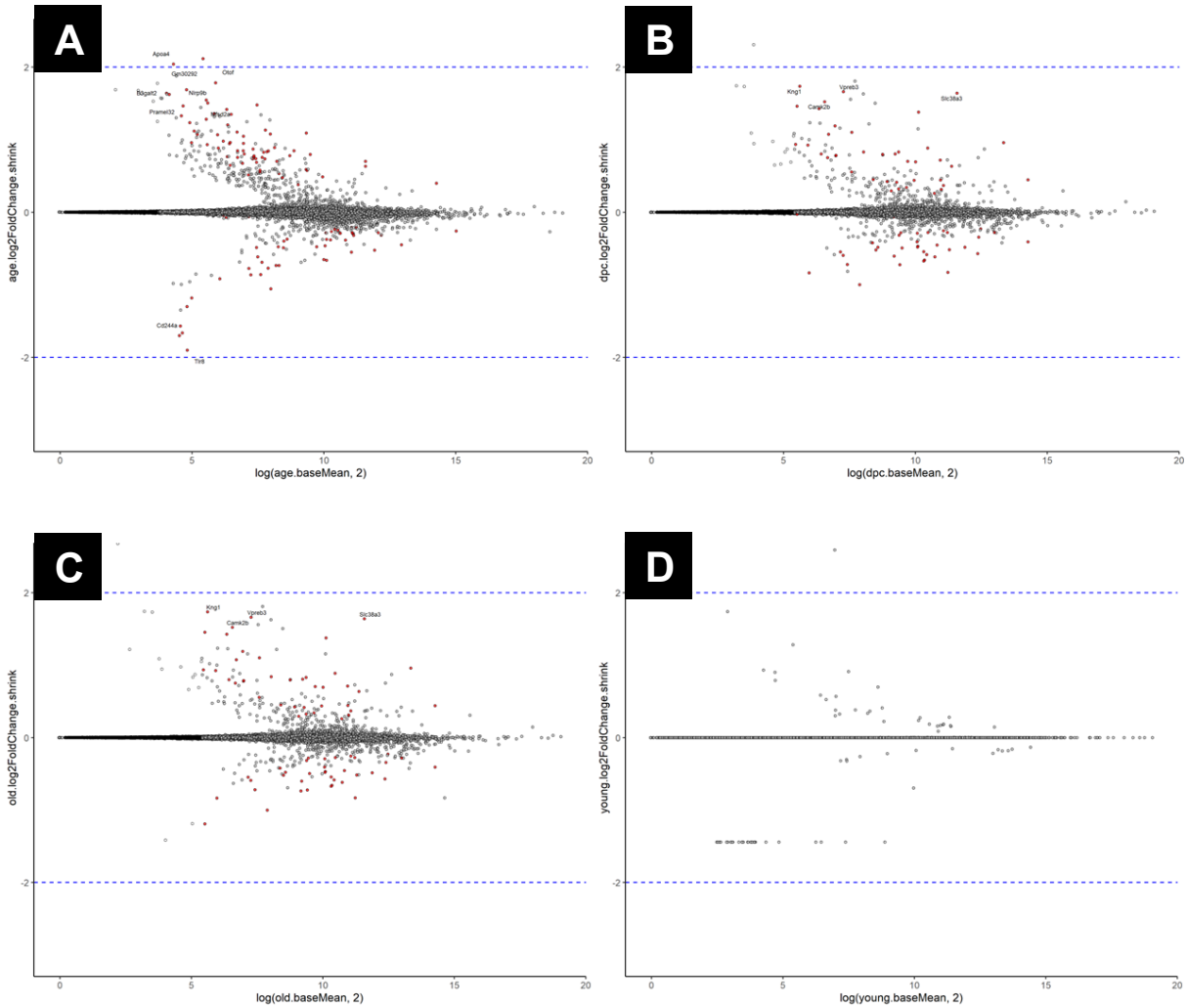

Figure 5. MA plots show the shrunken LFC value M (y-axis) plotted against the average expression across all samples A (x-axis) per gene. **A** Comparison of samples grouped by age. **B** Comparison of pooled age cohorts grouped by pregnancy stage. **C** Comparison between pregnancy stages within old cohort (O15.5 vs. O17.5). **D** Comparison between pregnancy stages within young cohort (Y15.5 vs. Y17.5). *Dotted line: LFC = 2, Red dots: Genes with* $p_{adj} < 0.05$.

To explore, whether there is a systemic relationship between the magnitude of gene expression and its differential expression among samples, we used “MA” plots, which compare the binary logarithm of sample gene expression values (M) to the average gene expression value across all samples per gene (A). When we averaged samples of the same age, gene expression differences scaled inversely with gene expression level and there was a slight trend of relative gene expression increase with age. Equally low numbers of genes were significantly upregulated and downregulated (Fig. 5A).

When averaging samples of the same time points, gene expression differences between 15.5 dpc and 17.5 dpc scaled inversely with gene expression level, following a similar but weaker pattern as the age comparison. The total number of significantly differentially regulated genes was similar as well. Between time points, there were fewer genes with strong expression decrease than between ages (Fig. 5AB). A separate comparison of Y15.5 and Y17.5 mice showed that very few genes change expression between time points in young mice, regardless of expression level (Fig.

6D). Indeed, after correction for multiple testing, we could detect no significant expression change between Y15.5 and Y17.5. In old mice, a total of 35 genes were (significantly) upregulated (with LFC ≥ 0.5 for 24 genes) and 38 downregulated (with LFC ≤ -(0.5) for 18 genes). In age comparison, 61 genes were upregulated in old mice (with LFC ≥ 0.5 for 58 genes) and 46 were downregulated (with LFC ≤ -(0.5) for 18 genes).

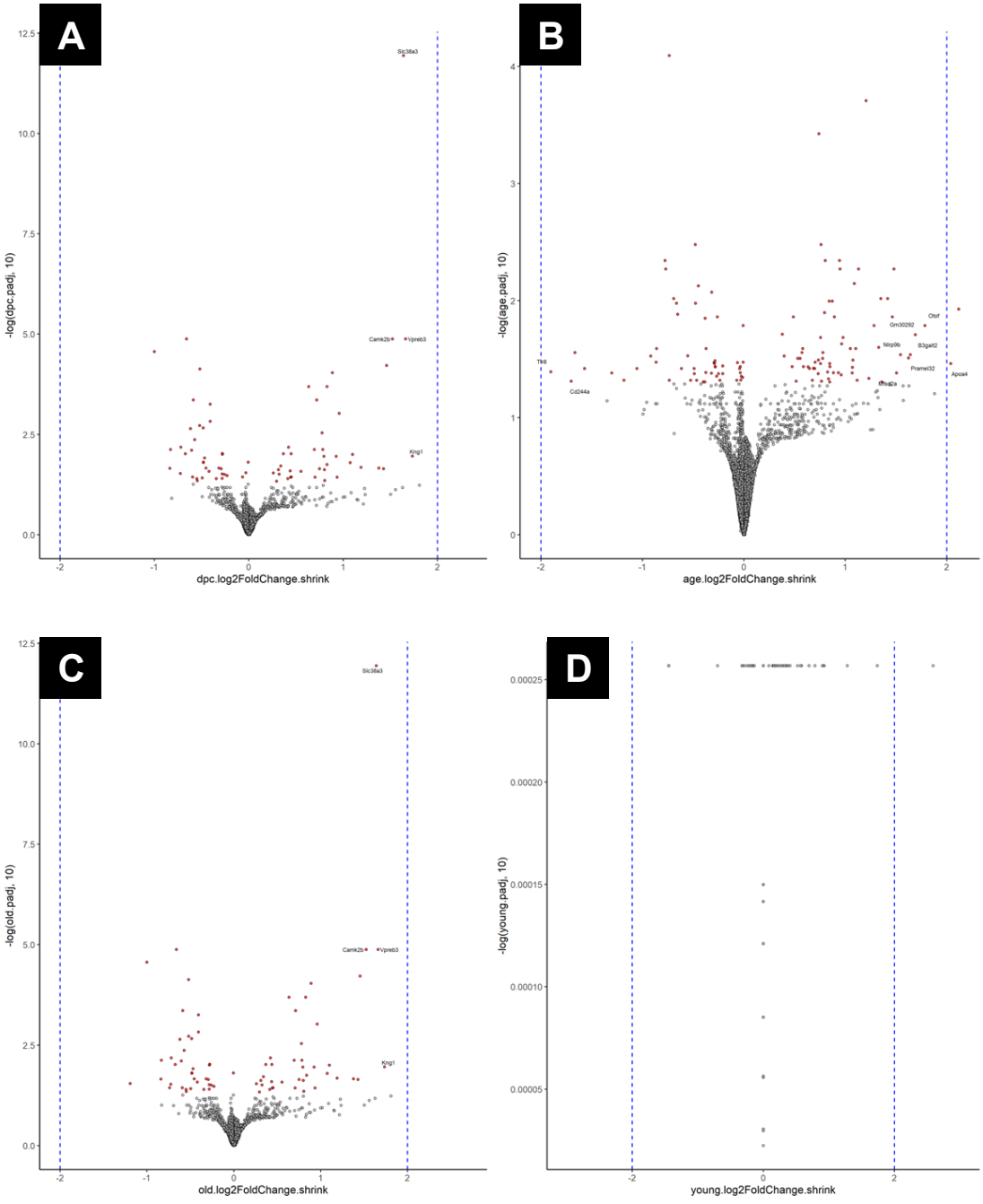

Figure 6. Volcano plots showing degree of significance (-Log_{10} of $p_{adjusted}$) on y-axis, and differential expression (shrunken LFC value) on x-axis, for every gene. **A** Differential expression refers to the comparison of all 15.5 dpc to all 17.5 dpc samples. **B** Differential expression refers to the comparison of all young to all old samples. **C** Comparison of O15.5 and O17.5. **D** Comparison of Y15.5 and Y17.5. *Dotted line: LFC = 2, Red dots: Genes with* $p_{adjusted} < 0.05$.

4.2 Expression of luteolysis-associated genes is subject to individual variation and does not change significantly from 15.5 dpc to 17.5 dpc

Table 1. Genes with shrunken LFC value greater than 0.3 or lesser than - 0.3 in the Y17.5 cohort compared to the Y15.5 cohort. LFC values are shrunken using *apeglm* to account for genes with high dispersion. Note that adjusted p-values after Benjamini-Hochberg FDR correction have the same value for all expressed genes.

Gene	adjusted p-value	LFC_{shrink} from Y15.5 to Y17.5
Egr3	0.9994	2.59
Gjb2	0.9994	1.74
Arc	0.9994	1.28
Rbp4	0.9994	0.91
Trpm5	0.9994	0.90
Csf2rb	0.9994	0.70
Npb	0.9994	0.58
Scnn1a	0.9994	0.57
Adcyap1r1	0.9994	0.52
Bhlhe40	0.9994	0.41
Reno1	0.9994	0.38
Ttll3	0.9994	0.37
Snai1	0.9994	0.36
Hs3st6	0.9994	0.30
Cks2	0.9994	- 0.30
Herc6	0.9994	- 0.32
Micu3	0.9994	- 0.33
Apln	0.9994	- 0.70

We next analysed the expression change of the genes of interest (GOI), identified by the literature and GO-term searches. Expression of most of the 65 genes, identified as associated with luteolysis, does not change in the corpora lutea of young mice between the 15.5 and 17.5 dpc. The PGF2α receptor *Ptgfr* was highly expressed at both timepoints, as was Prxl2b, the enzyme catalyzing the reduction of PGH2 to PGF2α (Fig. 8A) (Moriuchi et al. 2008). Expression of oxytocin receptor, *Oxtr*, was also elevated. *Oxtr*, expression of which is inhibited by P4, triggers myometrial contractions in presence of Oxytocin, and may be involved in regulation of PGF2α synthesis (Fuchs et al. 1995, Fang et al. 1997, Sugimoto et al. 1998). The investigated PGF2α-signaling

targets (e.g. *Vegfa, Slit1, Robo2, Akr1c18* and *Hsd3b1*) are all expressed, but unchanged between Y15.5 and Y17.5. *Vegfa*, an important factor during luteolysis induction, is highly expressed at both time points (Fig. 8B) (Girsh & Dekel 2002, Wada et al. 2013). The genes involved in P4 synthesis and P4 catabolism are equally unchanged. *Hsd3b1*, which catalyzes the conversion of pregnenolone to P4, is very highly expressed at both time points (Dumont et al. 1992, McLean et al. 1995). Alltogether, gene expression of only 22 out of 20324 genes could be detected as changed in corpora lutea of young mice from early to late timepoint (i.e., having shrunken LFC of > 0.3 or < -0.3)), so that enrichment analyses were omitted. These genes are listed in Table 1; they are neither known to be functionally connected to luteolysis nor to each other.

The consistency in expression of most GOIs between time points is similar in old mice. As in young mice, *Vegfa*, *Ptgfr*, Oxtr and *Hsd3b1* are strongly expressed (Fig. 8A). The expression change in two genes is interesting. First, expression of *Hpgd*, which catabolizes prostaglandins, is significantly decreased in old mice compared to young mice (padj = 0,032; shrunken LFC = -1.28) (Okita & Okita 1996, Roizen et al. 2008) (Fig. 8). Second, the expression level of *Akr1c18* decreases in old mice compared to young mice (Fig. 8C). *Akr1c18* codes for 20alphaHSD, the primary enzyme responsible for P4 inactivation, and shown to have a crucial role in PGF2α-signaling-induced luteolysis.

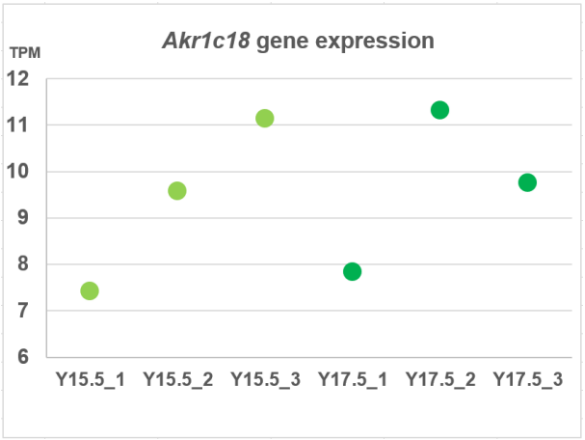

Figure 7. *Akr1c18* expression levels of Y15.5 and Y17.5 corpus luteum samples. Expression values are in transcripts per kilobase million (TPM).

We addressed the expression of Akr1c18 in more detail. Notably, gene expression values of *Akr1c18* were highly dispersed across samples of the same cohort, meaning there was high read count variability between biological replicates (Fig. 7). This variability can lead to overestimation of LFC values and noisy LFC estimates in general, which can compromise differential expression testing accuracy (Love et al. 2014, Zhu et al. 2019). To address this, we used the apeglm shrinkage estimator from the R-package apeglm in the DESeq2 function lfcshrink to shrink LFC estimates for genes with extremely high dispersion values, relative to genes of similar expression levels and lower dispersion. This gives a much lower LFC value for Akr1c18 (LFC_{age} = -1.41, LFC_{age_shrink} = 0.00154)

Given the observation of high heterogeneity in gene expression variance among Y17.5 samples, we looked into this aspect more closely (Piekorz et al. 2005, Mejia et al. 2015, Kapfhamer et al. 2018). Compared to the coefficient of variation (CV) in expression

values, averaged across all expressed genes, the coefficient of variation averaged across the 31 genes of interest involved in PGF2α-signaling, P4 synthesis and P4 catabolism is high (0.045 , relative to 0.014 for all expressed genes). Of these, 22 (9) genes of interest have an above-average (below-average) variance (Tab. 2). Most strikingly, the CV of *Akr1c18* is the highest of any gene (0.181). Furthermore, four out of the ten genes with highest CV (*Akr1c18*, *Cyp17a1*, *Hsd17b1* and *Inha*) are involved in murine luteolysis. *Cyp17a1* and *Hsd17b1* are, like *Akr1c18*, involved in P4 catabolism (Waite et al. 2016, Yoshimoto et al. 2016). *Inha*, coding for Inhibin A, has been identified as a target of PGF2α-signaling (Waite et al. 2016, Walton et al. 2022). Two more, *Inhba* and *Inhbb*, coding for Inhibin B, have been shown to regulate FSH-synthesis in the pituitary and the apoptosis of ovarian granulosa cells (Bao et al. 2021). For 20 out of 31 GOI, the individual Y17.5_2 has either the highest or the lowest expression value of all six young mice sequenced (Tab. 2). The increased variation among the Y17.5 replicates is driven by 17.5_2. This could indicate rapidly changing expression values in a specific group of genes at this pregnancy stage, and reveal a signature of starting luteolysis in Y17.5_2.

Table 2. Gene expression data of GOI with direct involvement in luteolysis. Mean gene expression levels in young mice and gene expression level of the individual Y17.5_2 are shown, as GOI expression in the latter deviates strongly from the other samples of the same cohort. Expression values are vst-normalized and log-transformed to allow for acute within-sample comparisons (Anders & Huber 2010). *(Gene in brackets) = Involvement in non-rodent luteolysis is proven, but involvement in rodent luteolysis is putative. Bold = Highest expression value of all young mice. Underlined = Lowest expression value of all young mice.*

Gene	Process *"+": enhance* *"-": inhibit*	Mean expression in TPM	Y17.5_2 expression in TPM	CV (Y17.5 samples)
Akr1c18	P4 catabolism +	9.50	**11.31**	0.181
Cyp17a1	P4 catabolism +	9.52	**10.72**	0.124
(*Inhba*)	(Luteal apoptosis +)	(11.80)	(**12.82**)	(0.097)
Hsd17b1	P4 catabolism +	10.44	**11.14**	0.082
Inha	PGF2α signaling +	13.28	**14.18**	0.074
Oxtr	PGF2α synthesis +	11.65	10.71	0.069
Egr1	(PGF2α signaling +)	10.13	10.26	0.066
(*Inhbb*)	(Luteal apoptosis +)	(11.91)	(**12.55**)	(0.062)
Hpgd	PGF2α synthesis -	9.02	**9.49**	0.056
Slit2	Luteal apoptosis +	8.77	8.44	0.045
Akr1c20	P4 catabolism +	7.29	**7.51**	0.030
Vegfa	PGF2α signaling +	13.61	13.26	0.026

(*Fgf2*)	(PGF2α signaling +)	(9.05)	(9.22)	(0.023)
Parm1	P4 catabolism -	11.67	11.27	0.022
Edn1	PGF2α signaling +	7.66	**7.82**	0.020
Egfr	PGF2α synthesis -	10.63	10.39	0.019
Prxl2b	PGF2α synthesis +	10.82	10.58	0.019
Ednrb	PGF2α signaling +	10.72	**10.92**	0.018
Lhcgr	PGF2α signaling -	14.66	14.35	0.018
Casp3	Luteal apoptosis +	10.01	9.86	0.018
Ptgfr	PGF2α signaling +	14.52	14.13	0.016
Scp2	P4 synthesis +	11.74	11.52	0.014
Nr5a1	P4 catabolism +	11.82	**12.01**	0.014
Egf	PGF2α synthesis -	7.82	7.58	0.013
Hsd3b1	P4 synthesis +	16.89	16.65	0.010
Casp8	Luteal apoptosis +	9.38	9.31	0.009
Robo1	Luteal apoptosis +	10.27	10.24	0.007
Ptgs1	PGF2α synthesis +	7.96	8.00	0.007
Stard3	P4 synthesis +	9.62	9.66	0.005
Ednra	PGF2α signaling +	9.78	9.78	0.005
Yy1	P4 synthesis -	11.13	11.16	0.002

4.3 Immune system genes are upregulated as proliferation declines in CL of old mice

Using PANTHER and GOrilla, we detected no significantly enriched biological process with pregnancy progression in old mice. However these tools rely heavily on how the GO terms are populated. To understand, what processes the detected differentially expressed genes are related to, we therefore examined the genes with significant and strong expression change in old mice individually. The twenty genes with the strongest expression decrease ($-1.2 \leq LFC_{shrink} \leq -0.57$) are structural cell components (*Tubb2b*, *Col11a2* and *Tmem132a*), immune response mediators (*H2q7*, *Ptk2b* and *Trfsrf9*, which is also pro-inflammatory), a pro-apoptotic protease (C2), a myelin component negatively affected by autophagy (*Pmp22*) (Gullstrand et al. 2009, Fortun et al. 2007, Yu et al. 2022), and 12 more genes we could not relate to each other nor to processes obviously relevant to luteolysis or the ovary (Tab. 3). Six of the 25 genes with the strongest expression increase ($1.74 \geq LFC_{shrink} \geq 0.57$) have immune function, *Kng1*, *Camk2*, *Zcchc12*, *Lrrc33*, *Fcna* and *Vpreb3*; the other 19 genes are not obviously related to each other or to relevant processes (Tab. 3). When comparing the pregnancy

progression-related CL gene expression changes in aged mice to those of the young mice, the GOrilla search using genes ranked by magnitude of gene expression change yielded significant under-representation of two processes in old mice, the cell cycle (p_{adj} = 0.00117) and cell division (p_{adj} = 0.00867). Correspondingly, using PANTHER for the same purpose, we found 11 biological processes related to cell cycle and proliferation (7 mitosis-related, 2 meiosis-related and 2 DNA replication-related) to be under-represented in old mice. Both GOrilla and PANTHER also found multiple over-represented processes involved in immune system function (namely “positive regulation of immune response”, “leucocyte differentiation”, “T cell differentiation”, ”T cell activation” and “regulation of lymphocyte differentiation”) in old mice.

Table 3. Genes with the strongest expression change between old and young mice. The p-values given are corrected for multiple testing using Benjamini-Hochberg, LFC values are shrunken using apeglm to account for genes with high dispersion.

Gene	p-value	LFC_{shrink} in Old compared to Young
Kng1	0.011	1.74
Vpreb3	$1.3 * 10^{-5}$	1.66
Slc38a3	$1.1 * 10^{-12}$	1.65
Camk2b	$1.3 * 10^{-5}$	1.52
Zcchc12	$6.0 * 10^{-5}$	1.46
Gm4813	0.023	1.43
Apof	0.022	1.38
Ankfn1	0.021	1.19
Acpp	0.010	1.10
Lrrc3	0.016	1.07
Gng12	$9.4 * 10^{-4}$	0.96
Fcna	0.037	0.94
Clec1b	0.011	0.93
Znhit6	$9.1 * 10^{-5}$	0.89
Nnat	$2.0 * 10^{-4}$	0.83
Dsc2	0.045	0.81
Npb	0.024	0.80
Sema3e	0.011	0.80
Hs3st6	0.008	0.78
Fgfbp3	0.003	0.78

Tiparp	$4.4 * 10^{-4}$	0.71
Tmem141	0.037	0.70
Stat5a	0.008	0.69
Chst11	$2.0 * 10^{-4}$	0.64
Zfp711	0.026	0.56
Aldh1b1	0.002	- 0.52
Plxnb1	0.045	- 0.52
Dok3	0.040	- 0.55
Kcnk3	0.004	- 0.55
Efhd1	$4.4 * 10^{-4}$	- 0.57
C2	0.036	- 0.59
Susd3	0.008	- 0.60
Tnfrsf9	0.002	- 0.60
Pmp22	$1.3 * 10^{-5}$	- 0.61
Tmem132a	0.010	- 0.66
Gm9899	0.007	- 0.67
Ptk2b	0.030	- 0.72
H2-Q7	0.036	- 0.72
Rnf180	0.007	- 0.74
Col11a2	$2.7 * 10^{-5}$	- 0.83
Tubb2b	0.029	- 1.00

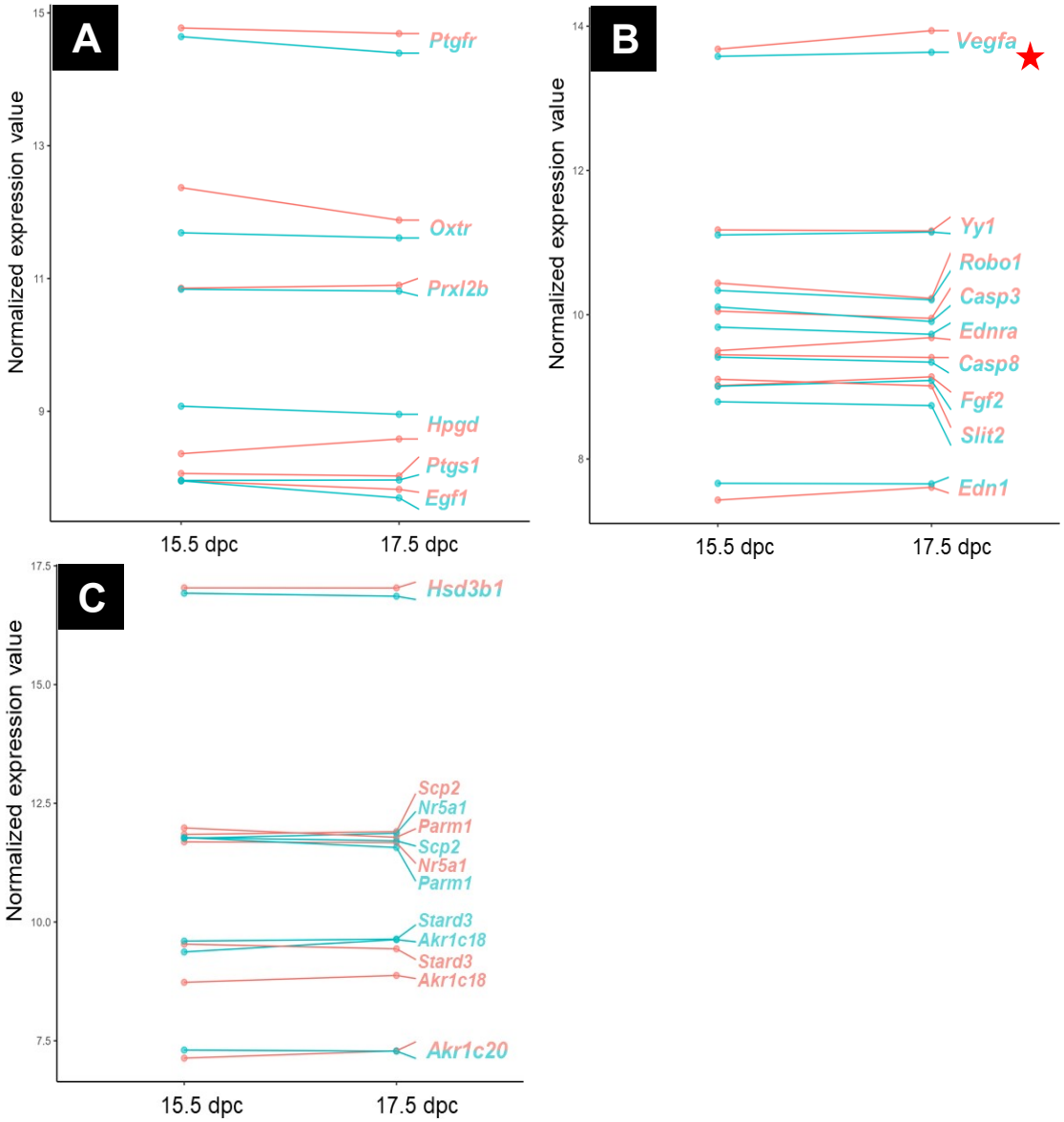

Figure 8: Expression trends of selected GOI in young mice (Blue) and old mice (Red). Averages across 3 replicates are shown. **A** Genes with central role in PGF2α synthesis, regulation and signal transduction. **B** Main targets of *PTGFR*-signaling in the corpus luteum. **C** Main components of Progesterone synthesis, inhibition and degradation. *Red star: significant (p_{adj} < 0.05) expression difference.*

4.4 Peripheral blood hormonal levels at 17.5 do not forecast the Upcoming luteolysis

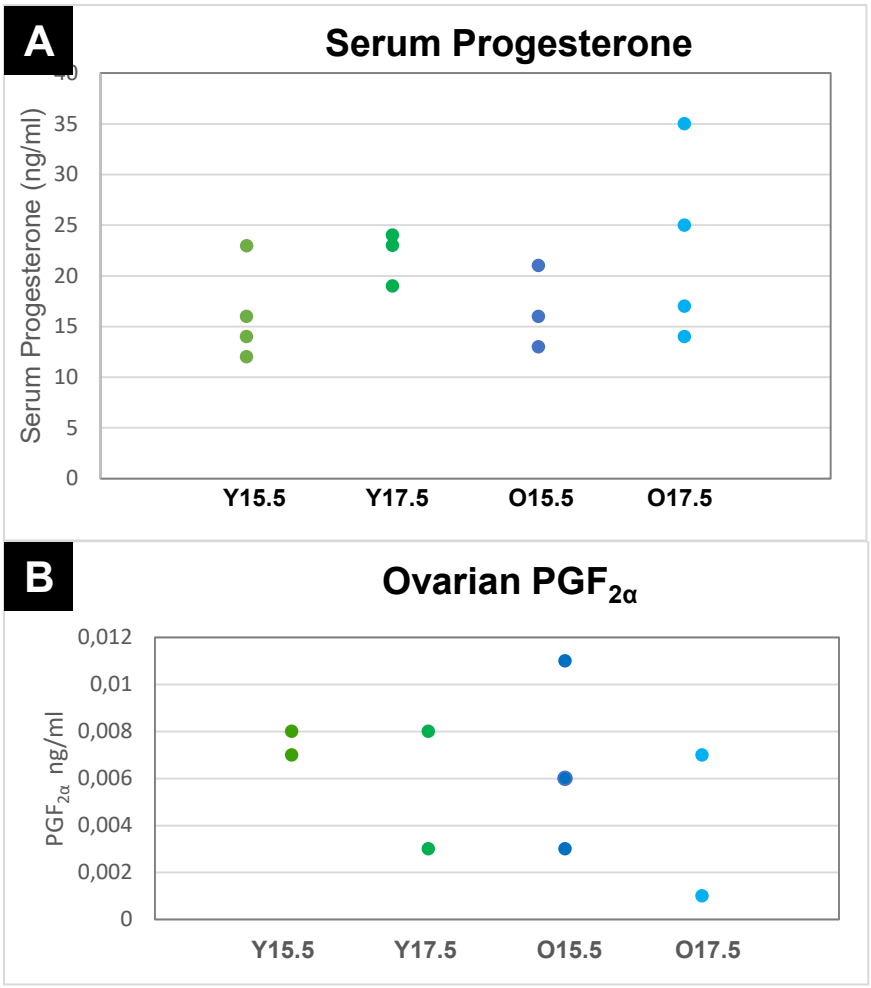

Figure 9. **A** Progesterone measured in peripheral blood serum. **B** $PGF_2\alpha$ measurements from homogenized CL tissue.

We have also measured progesterone levels in peripheral blood in three (4) individuals per age group and pregnancy stage, to see whether the progesterone has started to decline in the later stage, a characteristic of luteolysis. Mean serum Progesterone measurements at 17.5 dpc were nominally higher at both ages compared to 15.5 dpc (Fig. 9A). However, the difference between time points was not significant as the variance of these measurements is known to be quite high (young mice: $p = 0.07$; old mice: $p = 0.17$). There was also no significant overall difference between ages ($p = 0.68$) and dpc ($p = 0.07$) (Tab. 4). We furthermore assessed the levels of local PGF2α in corpus luteum tissue, and confirmed that the levels are very low and there is no systematic difference between stages nor between age groups (Fig. 9B, Tab. 4).

Table 4. Steroid hormone measurements and significance tests for group differences.

	P4 in ng/ml MEAN **(SD)**	**PGF2A** in ng/ml MEAN **(SD)**
Y15.5	16.3 (4.9)	$7.5 * 10^{-3}$ ($0.7 * 10^{-3}$)
Y17.5	21.9 (2.9)	$5.5 * 10^{-3}$ ($3.5 * 10^{-3}$)
O15.5	16.7 (4.0)	$6.6 * 10^{-3}$ ($4.0 * 10^{-3}$)
O17.5	22.8 (9.4)	$4.0 * 10^{-3}$ ($4.2 * 10^{-3}$)

young	18.7 (4.8)	$6.5 * 10^{-3}$ ($2.4 * 10^{-3}$)
old	20.1 (7.8)	$5.6 * 10^{-3}$ ($3.8 * 10^{-3}$)
15.5 dpc	16.4 (4.1)	$7.0 * 10^{-3}$ ($2.9 * 10^{-3}$)
17.5 dpc	22.4 (6.8)	$4.8 * 10^{-3}$ ($3.3 * 10^{-3}$)
Student's *t*-test for **P4**		
	t-value (DF)	p-value
Y17.5 vs. Y15.5	1.7 (5)	0.07
O17.5 vs. O15.5	1.0 (5)	0.17
old vs. young	0.41 (6)	0.68
17.5 dpc vs. 15.5 dpc	1.99 (6)	0.07
Student's *t*-test for PGF2A		
	t-value (DF)	p-value
Y17.5 vs. Y15.5	0.78 (2)	0.51
O17.5 vs. O15.5	0.71 (3)	0.53
old vs. young	0.41 (7)	0.70
17.5 dpc vs. 15.5 dpc	1.09 (7)	0.16

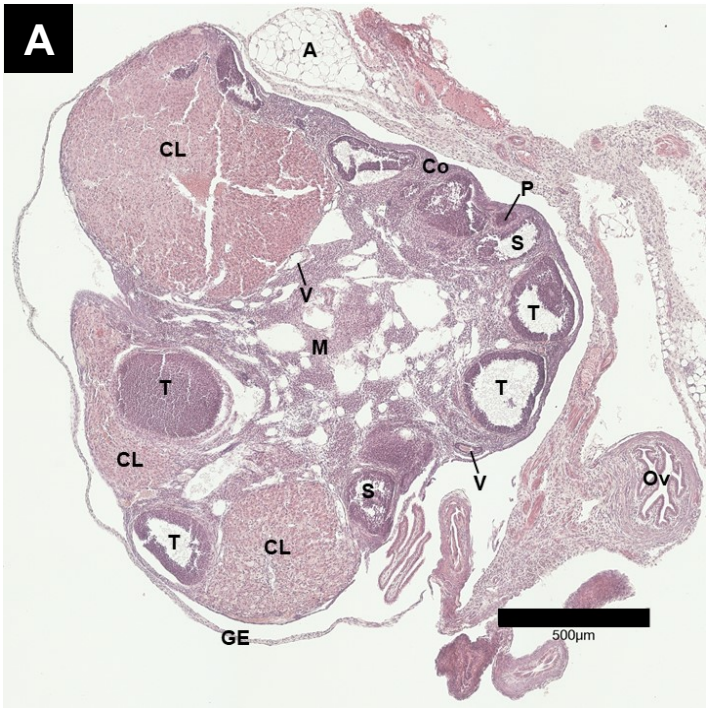

Figure 10. Y17.5 Ovary stained with Hematoxylin and Eosin. **A** Overview (10x). **B** Corpus luteum (20x). *A: Adipose tissue, CL: Corpus luteum, Co: Cortex, E: Erythrocytes, GLC: Granulosa Lutein Cells, M: Medulla, Ov: Oviduct, P: Primary Follicle, S: Secondary Follicle, T: Tertiary Follicle, TLC: Theca Lutein Cells, GE: Germinal Epithelium, V = Blood Vessel. Scale bars = 500 µm.*

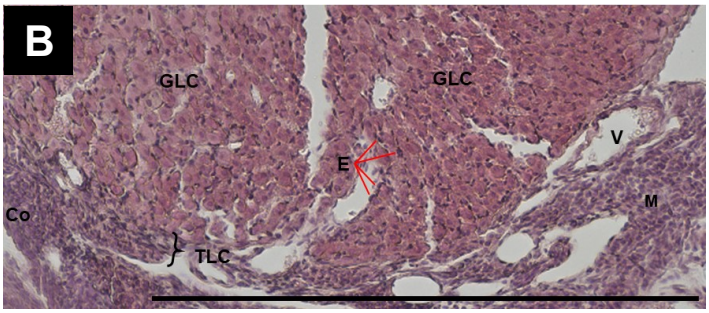

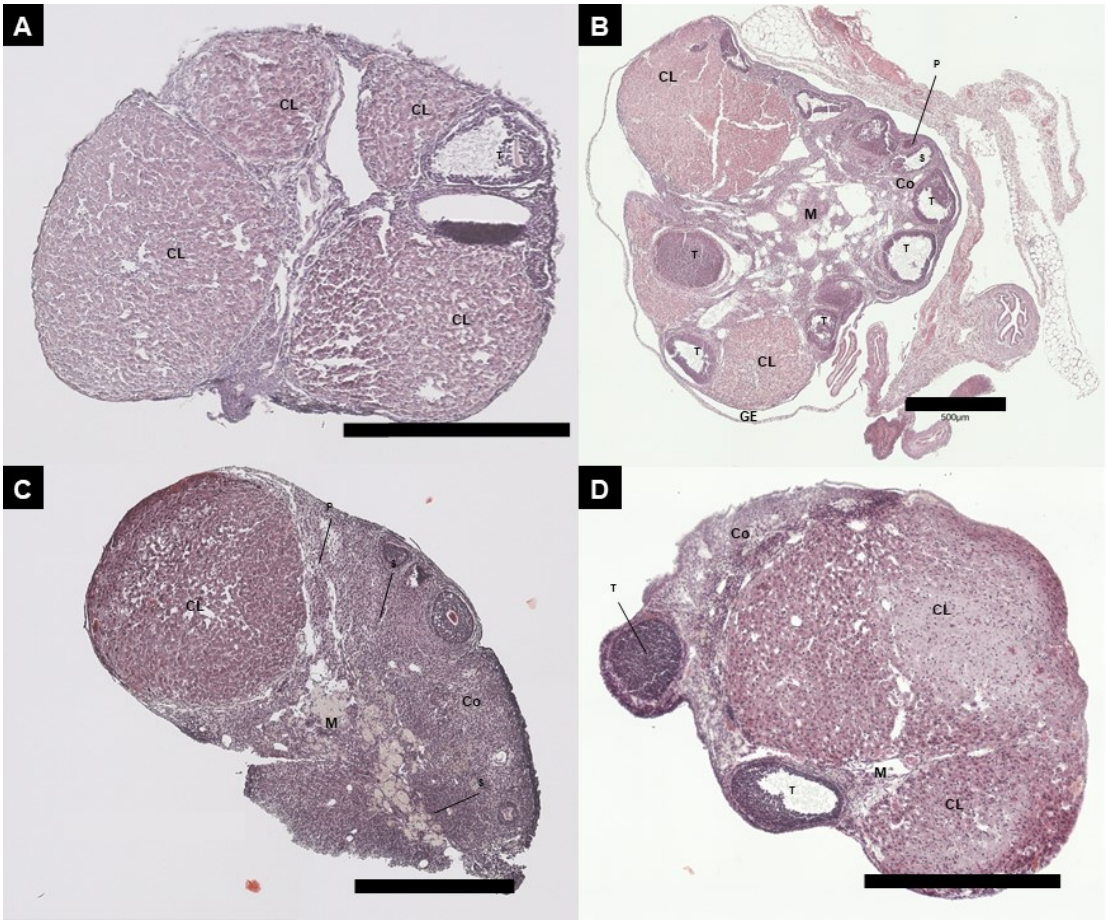

Figure 11. Ovaries stained with Hematoxylin and Eosin (10x). **A** Young 15.5 dpc. **B** Young 17.5 dpc. **C** Old 15.5 dpc. **D** Old 17.5 dpc. *A: Adipose tissue, CL: Corpus luteum, Co: Cortex, M: Medulla, Ov: Oviduct, P: Primary Follicle, S: Secondary Follicle, T: Tertiary Follicle, GE: Germinal Epithelium, V = Blood Vessel. Scale Bars = 500 µm.*

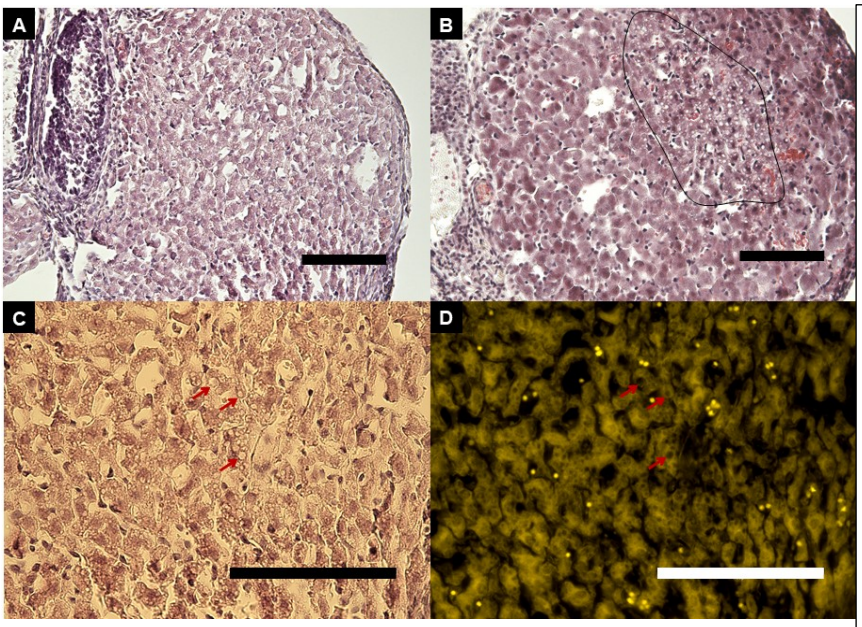

Figure 12. Granulosa lutein cells exhibiting cytoplasmic vacuolation at 15.5 dpc in young (**A, C, D**) and old (**B**) mice (H&E Stain). **B** Healthy GLCs surrounding a cluster of deformed GLCs with heavily vacuolated cytoplasm (encircled). **A, C** Mostly deformed GLCs with heavily vacuolated cytoplasm. **D** Differential autofluorescence enhances visualization of individual cells. Vacuoles are contained within, not between, individual GLCs. *Scale bars = 100 µm. Red arrows = Vacuoles contained within cells*

4.5 Morphological differences between the 3-month old and 8-month old late pregnant ovary

Late-phase ovarian morphology of both age groups is consistent with previous descriptions of late pregnancy. Roughly half of the ovarian tissue is filled with corpora lutea, the largest structures in the ovary with a diameter of up to 900 µm each (Fig. 11). They are made up of a thin outer layer of theca lutein cells encompassing larger (~20 µm) granulosa lutein cells (GLCs), both of which are stained in intense pink in H&E due to their cytoplasm being strongly stained with Eosin (Fig. 10 B). They are interspersed with capillaries and smaller cells, erythrocytes, which stain dark purple in H&E (Fig. 10 B). The second largest and most abundant structures are developing follicles, more strongly stained with hematoxylin due to the higher density of nuclei related to the non-hypertrophic cytoplasm and ECM, giving them an altogether darker blue appearance in the stained ovary. Depending on the stage of folliculogenesis, they measure between 50 µm (primary follicles) and 350 µm (tertiary follicles). The follicles are surrounded by connective tissue of the ovarian cortex. The connective tissue in the center of the ovary, the medulla, seems to contain more blood vessels than the cortex. A portion of the GLCs exhibit marked cytoplasmic vacuolation in all samples; this is apparent in roughly half of the CL in each ovary. The non-vacuolated GLCs are roundish and measure about 20 µm in diameter (Fig. 10 B & 11 B). The GLCs with vacuolated cytoplasm have mostly lost this shape; they are smaller and many of them appear flattened or stretched (Fig. 12 D). In one individual (Y17.5_2) we observed a densely packed cell mass in the center of the CL (Fig. 13). The surrounding GLCs are

interspersed with erythrocytes. The dense cell mass has similar fluorescent properties, suggesting that it is a clump of erythrocytes. (Fig. 13 CD). Cell membranes in this cell mass seem to still be intact as the cell borders are still visible, but there are no visible nuclei; this also points to erythrocytes, as they are the only non-nucleated cells in mammals (Fig. 13 D).

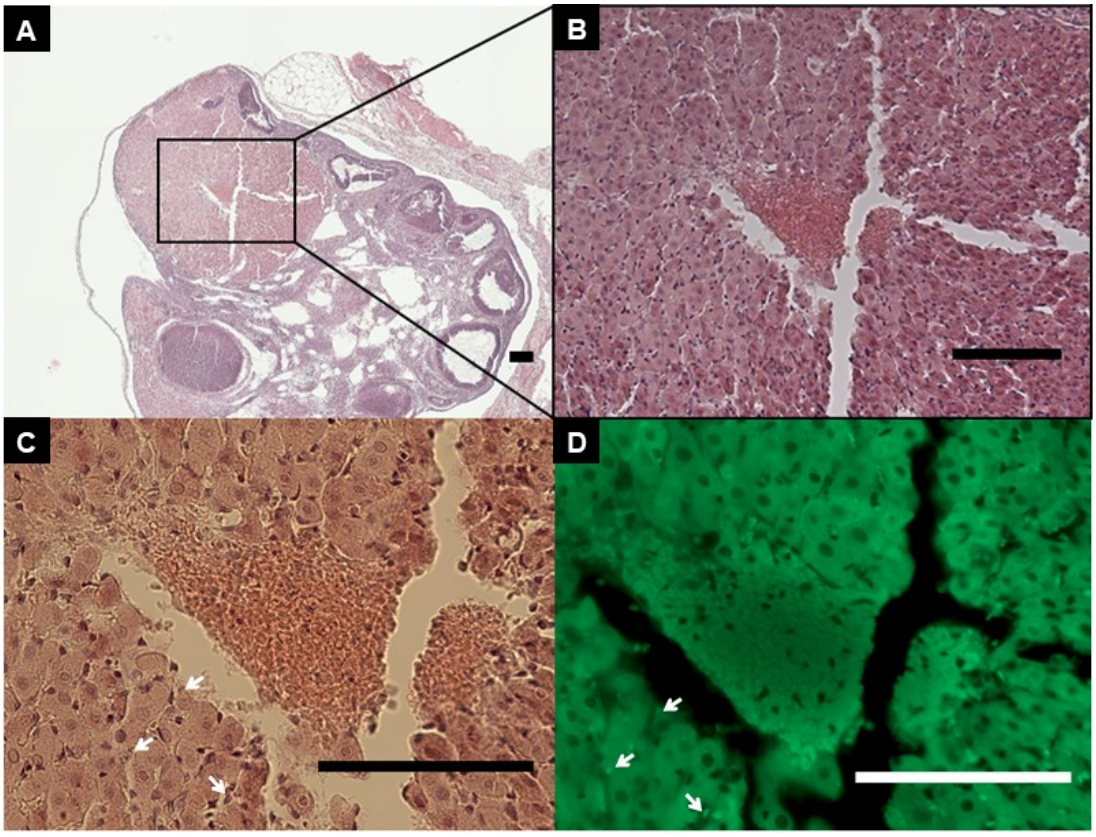

Figure 13. Corpus luteum of Y17.5_2 (H&E stain). **A** Ovary overview (10x). **B-D** Center of corpus luteum showing coagulative necrosis in brightfield (**B,C** 20x,40x) and autoflourescence captured in green channel (**D**, 40x) imaging. Note that the erythrocytes show strong autofluorescence. *Scale bars: 100 µm. White arrows: Erythrocytes.*

4.6 The old ovarian medulla contains age pigments and accumulations of large, iron-filled cells

Staining with Perl's shows that there are clusters of large, circular cells in the medulla of old mice, containing ferric iron (Fig. 14/14). They range from faint to dark, intense Prussian blue staining, and all show strong fluorescence when excited at 482 nm wavelength (Fig. 15 E-H). Other cells with similar fluorescent properties, but more intense staining and less distinctive shape, were few and scattered, but were found consistently in both old and young medullae (Fig. 15, orange arrowheads). In contrast to both, some vesicles located within the large, circular cells in old samples are intensely stained, but lack fluorescent activity (Fig. 15, red arrowheads).

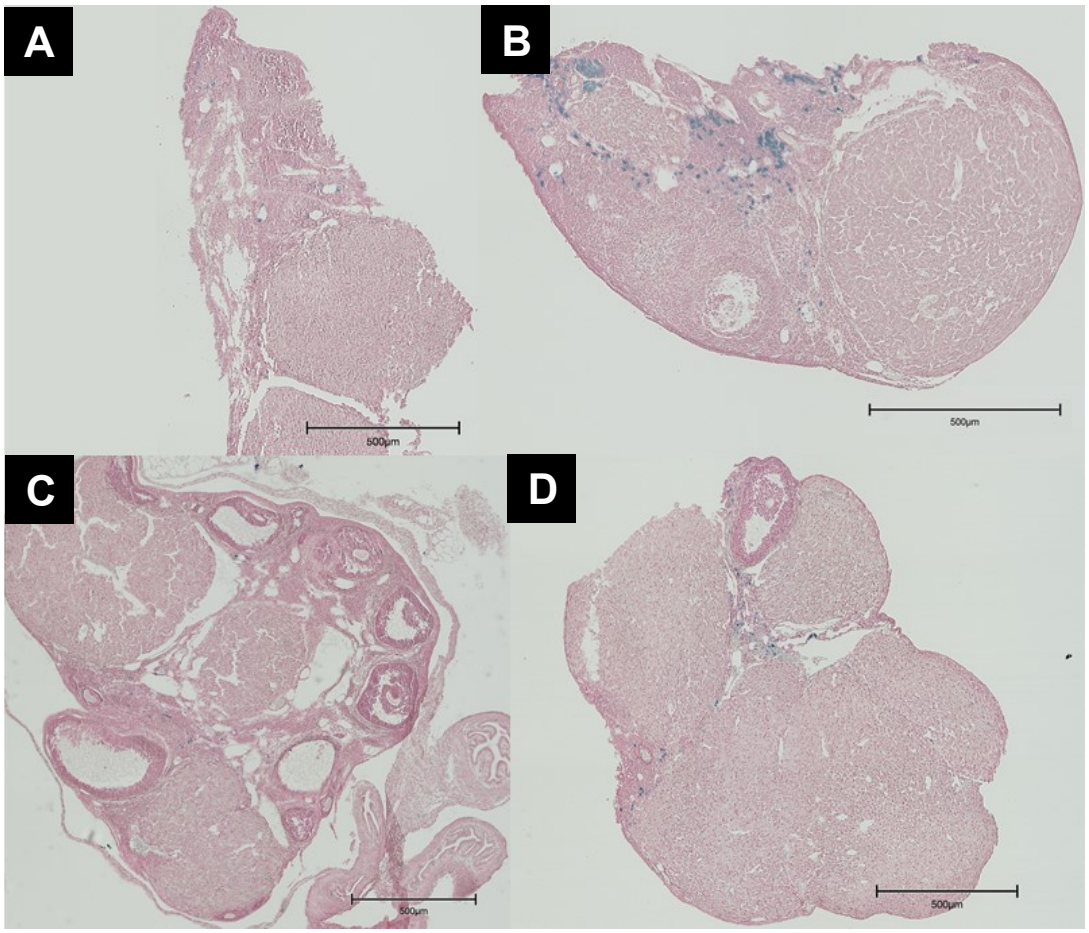

Figure 14. Ovaries stained with Perl's stain. **A** Young 15.5 dpc (10x). **B** Old 15.5 dpc (10x). **C** Young 17.5 dpc (10x). **D** Old 17.5 dpc (10x). *Scale bars = 500 µm.*

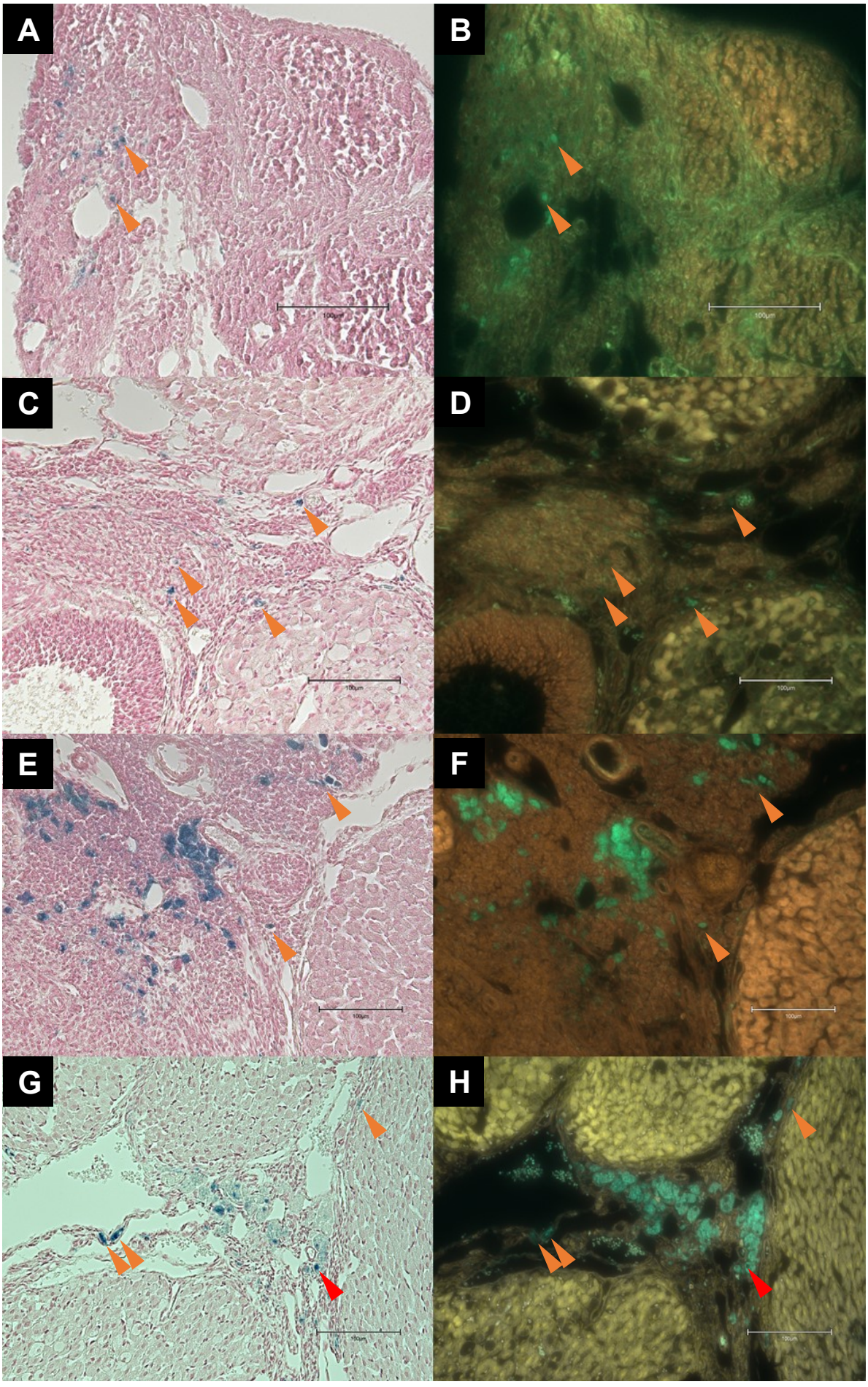
A
B
C
D
E
F
G
H

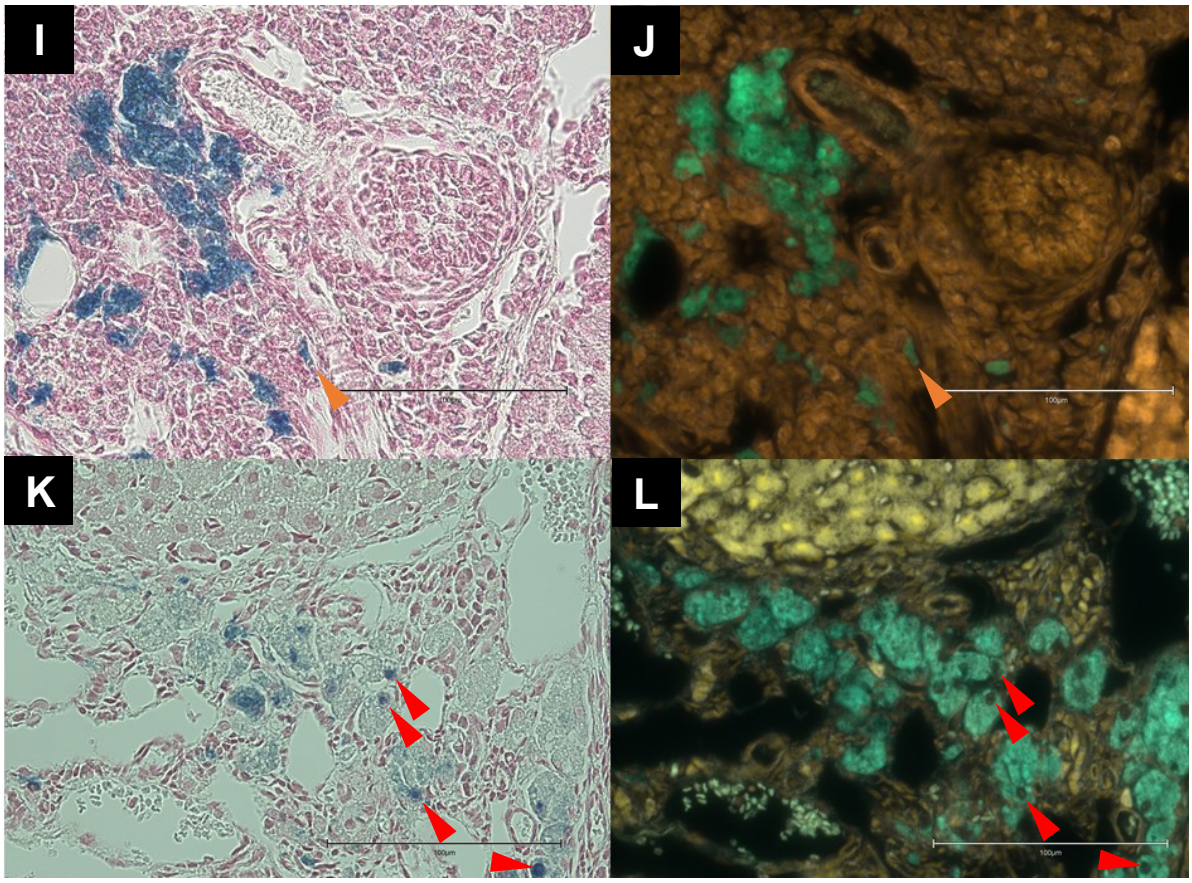

Figure 15. Ovaries stained with Perl's stain. Brightfield (left) and multi-channel fluorescence overlay of 482 nm (green) and 500 nm (yellow) excitation (right). GLCs show strong yellow autofluorescence, erythrocytes appear nearly white as they show strong yellow and weak green autofluorescence, and macrophages show strong green and weaker yellow autofluorescence, appearing teal or green. **AB** Young 15.5 dpc (20x). **CD** Young 17.5 dpc (20x). **EF** Old 15.5 dpc (20x). **GH** Old 17.5 dpc (20x). **IJ** Old 15.5 dpc (40x). **KL** Old 17.5 dpc (40x). *Scale bars = 100µm. Red arrowheads = Intensely stained vesicles lacking fluorescence. Orange arrowheads = Intensely stained cells showing fluorescence.*

5 Discussion

5.1 The CL of late murine pregnancy is characterized by autophagosome formation

We found histological signs of GLC autophagy in all samples. In each histologically examined ovary, some CL, but not all, had visible vacuoles. This could be an indicator of early luteolysis, as previous investigations found autophagy to be the first structural sign of luteolysis (Fraser et al. 1999, Vázquez-Nin et al. 2011). Luteolytic autophagy becomes visible as cytoplasmic vacuolation, the appearance of autophagic vacuoles of varying sizes. These vacuoles contain lipid droplets and cell organelle debris such as distorted mitochondria (Malven & Francis 1969, Koering & Kirton 1973, Archbald, Al-Bagdadi & Godke 1981, Singh et al. 1988). An investigation in rats found that PGF2α induces luteal autophagy, and that the accumulation of autophagosomes leads to an increase in luteal apoptosis, while the inhibition of autophagosome formation leads to a decrease in luteal apoptosis (Choi et al. 2011). However, the autophagic process can also have homeostatic function and is not necessarily part of a regression (Ryter et al.

2013). As we did not detect a drop in P4 levels even at 17.5 dpc, 48 hours after the detection of autophagosomes, it seems unlikely that they are a sign of structural luteolysis. Still, they are likely a sign of a CL primed for luteolysis, as their accumulation induces an increase in luteal apoptosis.

In one individual, we found a dense clump of opaque, eosinophil cells with no nucleus situated in the center of the CL (Fig. 13). The clump measures about 100 um and is visually similar to the observations of Sato et al. (2014), who investigated the structural characteristics of luteolysis in cycling Wistar Hannover rats. They identified this cell clump as coagulative necrosis. Histologically, coagulative necrosis is characterized by opaque, eosinophil cells that lack a nucleus, but have temporarily preserved cell outlines (Miller & Zachary 2017). However, while they found accumulations of phagocytotic macrophages surrounding the necrotic cells, we found none. Additionally, coagulative necrosis is caused by a lack of blood supply, which is not the case in our sample, as the GLCs are interspersed with erythrocytes and blood vessels are visible both in and adjacent to the same CL (Fig. 10B). It is more likely that the cell clump consists of erythrocytes. These also have histological characteristics matching those of the cell clump, as well as similar autofluorescent properties when excited at 482 nm (Fig. 13 D). In Deanesly's (1930) description of the histological changes of various murine CL stages, a CL with a similar central cell mass can be seen in post-partum mice. Deanesly described this appearance as a transitional condition between the CL of pregnancy and the CL of lactation, but stopped short of describing the structure in more detail (Deanesly 1930). Unfortunately, we could not find a proper histological description of early structural luteolysis in mice; most histological investigations of luteolysis in rodents to date have been conducted in hamsters or rats (Malven & Francis 1969, Paavola 1979, Greenwald 1986). It is difficult to make inferences from these investigations because the early stages of structural luteolysis vary considerably among, and even within, rodent species (Sugino & Akuda 2007, Sato et al. 2014). It is unclear what this likely erythrocyte aggregation means, but it may be connected to luteolysis if it is indeed the same condition previously observed in post-partum mice (Deanesly 1930).

5.2 Systemic progesterone withdrawal occurs after 17.5 dpc

Our P4 measurements indicate no functional luteolysis (decrease of P4 levels in serum). We did not find a change in serum P4 concentration between 15.5 dpc and 17.5 dpc. This does not correspond to previous studies; they all report a similar pattern, albeit absolute serum P4 concentration varies between studies. Sugimoto et al. (1998) observed a significant drop in serum P4 between comparable pregnancy stages, while Patel et al. (2017) and Pavlicev (unpublished) observed a pronounced drop between 15.5 dpc and 17.5 dpc. Interestingly, Patel et al. measured the strongest drop in serum P4 concentration between 17.5 dpc and 18.5 dpc. Thus, our data indicates that in the line studied here, a significant decline in systemic P4 occurs only after 17.5 dpc.

5.3 Individual variation in luteolysis timing may mask important trends in gene expression

In addition to high overall correlation between transcriptomes at two time points of pregnancy progression, we found no consistent upward trend in expression of the genes involved in PGF2α-signaling and P4 catabolism, and no downward trend in expression of the genes involved in P4 synthesis. The consistently high expression of the *Hsd3b1* gene, coding for the enzyme directly catalyzing the final P4 synthesis step, indicates that P4 synthesis is still fully active (Kadam et al. 1984, Bremer & Miller 2014). The continuous strong expression of the PGF2α-receptor *Ptgfr* matches previous reports on the timing of *Ptfgr* upregulation in mid-to late pregnancy, which also demonstrated that PTGFR is localized to lutein cell membranes (Sakamoto et al. 1995, Hasumoto et al. 1997). The genes with central functions in PGF2α-induced luteolysis show high individual variation in gene expression across our young samples at 17.5 dpc. In spite of the lack of general trend across samples, at closer inspection, one individual does show an interesting pattern of gene expression that is indicative of a beginning luteolysis: The individual Y17.5_2 not only has an extreme expression level within its age group for many (20 out of 31) of luteolysis-associated genes (Tab. 3), this deviation from the other young samples of the same cohort also shows an intriguing pattern. Y17.5_2 has the highest expression level of *Edn1*, a PGF2α-signaling target with putative role in luteolysis induction that is temporally associated with P4 withdrawal, and of its' receptor *Ednrb* (Milvae 2000, Stocco et al. 2001). It has the lowest expression level of *Vegfa*, an angiogenic factor downregulated by PGF2α in luteolysis (Tab. 2, Stocco et al. 2001). Moreover, Y17.5_2 has the highest expression level of the nuclear receptor *Nr4a1*, which is rapidly upregulated by PGF2α just before parturition in the mouse CL to transactivate the *Akr1c18* (20a-HSD) promoter (Stocco et al. 2000, 2002). Expression of the known P4 catabolism enzyme genes *Akr1c18, Akr1c20, Cyp17a1* and *Hsd17b1* is highest in Y17.5_2, and expression of the P4 catabolism inhibitor *Parm1* is lowest (Park et al. 2013). On the other hand, the components (*Slit2* and *Robo1*) and targets (*Casp3* and *Casp9*) of the PGF2α-induced Slit/Robo signaling pathway do not have elevated expression in Y17.5_2 compared to other samples. Expression of *Hsd3b1*, which catalyzes P4 synthesis, is lower than in the other young mice, albeit *Hsd3b1* is still highly expressed (Tab. 2). The expression of the P4 synthesis enhancer *Stard3* and of the P4 synthesis inhibitor *Yy1* show low individual variation, and no extreme value in Y17.5_2 (Liu et al. 2007, Clark & Stocco 2014). Interestingly, the expression level of *Hpgd*, which is activated by P4 to directly inactivate PGF2α, is also elevated in the Y17.5_2 individual.

Taken together, Y17.5_2 gene expression indicates higher activity of PGF2α signaling pathways. Genes active in PGF2α-induced P4 catabolism are upregulated compared to the other individuals from the same cohort. On the other hand, expression of luteal apoptosis genes is unaltered, and P4 synthesis is not clearly affected, by PGF2α signaling in Y17.5_2.

5.4 As Progesterone resists the destruction of its own production gland, activity of P4 synthesis and P4 catabolism is high at the same time

There are no definitive signs of structural luteolysis in our C57Bl/6 line at 17.5 dpc, and systemic P4 levels do not decline between 15.5 dpc and 17.5 dpc. There is neither differential expression of luteolysis genes between 15.5 dpc and 17.5 dpc in young mice nor between young and old mice. Still, the histological and transcriptomic data indicate a beginning withdrawal of P4 in the Y17.5_2 individual. The process of P4

withdrawal is a combination of P4 synthesis cessation and extant P4 catabolism, both induced by PGF2α signaling. While P4 synthesis is unaltered in Y17.5_2, P4 catabolism appears to be more active. We found autophagosome accumulations in all samples, possibly indicating that the CL are primed for luteolysis (Choi et al. 2011, Tang et al. 2017). This may be connected to the slighter initial drop in P4 levels starting around 14 - 15.5 dpc (strain-dependent), over three days before the dramatic P4 withdrawal caused by luteolysis (Murr et al. 1974, Patel et al. 2017, Edey et al. 2018). While Y17.5_2 does not have a lower systemic P4 level than the other Y17.5 individuals, measuring P4 in systemic blood serum may be inadequate when specifically investigating the onset of luteolysis due to a temporal difference in local and systemic P4 levels. A mechanism for local P4 withdrawal has been demonstrated in the myometrium and in cervix; this may also be the case in the ovary (Nadeem et al. 2021). P4 has an inhibitory effect on its own inactivation enzyme 20a-HSD (Sugino et al. 1997, Farina et al. 2004). In mouse luteolysis, PGF2α signaling increases both *Slit2* and *Robo1* expression. Slit/Robo signaling then leads to an increase in *Casp3* and *Casp9* expression, enhancing apoptosis of luteal cells (Zhang et al. 2013). P4 antagonizes this same process, decreasing the expression of *Slit2* and *Robo1* (Zhang et al. 2017).

Thus, we speculate that structural luteolysis and cessation of P4 production may occur near-simultaneously in mice, directly preceded by PGF2α-mediated increase in P4 catabolism. Furthermore, we speculate that murine luteolysis starts with local P4 withdrawal in the CL, preceding systemic P4 withdrawal. When the local P4 level starts to decline, production of 20a-HSD should increase as P4 activity decreases, in turn accelerating local P4 withdrawal and terminating inhibition of the Slit/Robo pathway and activating the luteal apoptosis cascade. At first, inactivation of PGF2α via *Hpgd* prevents luteolysis, but after a certain tipping point, local P4 withdrawal will increase exponentially, spreading through the whole CL. This would allow for a quick and coordinated involution of the transient gland, and potentially even induce local P4 withdrawal in neighboring CL.

5.5 Age-related accumulation of hemosiderin and enlarged macrophages in ovary occur at a younger age than previously thought

Gross ovarian morphology of old and young mice is similar. There is no clear morphological difference between the CL of old and young mice in late pregnancy. Cytoplasmic vacuolation is apparent at 15.5 dpc and 17.5 dpc in both age cohorts. However, we observed age-related morphological differences in the ovarian medulla. We found clusters of large, round, iron-laden cells in ovarian medullae of old mice. While we also observed a few iron-laden cells scattered in young mice, both their number and average size were much smaller (Fig. 15). The iron-laden cells found in old mice match previous descriptions, which identified them as clusters of enlarged macrophages (Asano 2012, Urzua et al. 2018). The most common term for these clusters is multi-nucleated giant cells, or MNGCs (Milde et al. 2015, Briley et al. 2016, Foley et al. 2021).

Asano (2012) compared ovarian morphology of non-pregnant C57Bl/6 mice of different reproductive ages (2, 3, 8, and 12 months of age) and found a steady increase in stromal ovoid macrophage abundance with age. In 12-month old mice, they found

clusters of enlarged macrophages (≥60 µm) which mirror the MNGCs in our 8-month old mice (Fig. 15 vs. Asano 2012/Fig. 3). Asano noted distinct intracellular non-heme iron accumulations in the enlarged macrophage clusters, concurrent with our observations (Fig. 15, red arrows). Urzua et al. (2018) investigated 20-month old murine ovaries identified these accumulations as intracellular hemosiderin granules. They also quantified hemosiderin accumulation and oxidative DNA damage, finding them to be directly proportional to one another. Hemosiderin initially stores excess iron safely, but when storage capacity is exceeded, the iron overload leads to redox-active iron, which damages leads to oxidative stress, damaging cell components and producing reactive oxygen species (Iancu et al. 1997, Reid et al. 2001, Galaris et al. 2019). Thus, it is likely that the ovaries of our old mice are subject to a higher degree of oxidative DNA damage than those of our young mice. Briley et al. (2016) investigated age differences in the ovarian stroma of CD1 mice and found MNGCs in most of the mice aged 10 months, but none in mice aged 4-7 months.

In sum, our observations add to the findings of previous studies on aging ovarian morphology. In our line, an age-related accumulation of hemosiderin-laden MNGCs in late pregnancy is visible at 8 months of age (Recalcati & Cairo 2021). Hemosiderin accumulations indicate an alteration in iron metabolism, which can lead to oxidative damage (Lancu 1990, Miyazaki et al. 2002, Wang et al. 2010, Dos Santos et al. 2022). The function of MNGC formation is not entirely clear. It has been suggested that the cells fuse to allow for phagocytosis of structures too large for single macrophages (McNally & Anderson 2005, Helming & Gordon 2009). They have been found in various inflammation processes, and are usually indicators of chronic inflammation (Clambers & Spector 1982, McNally & Anderson 2011, Milde et al. 2015). Thus, the age-associated formation of MNGCs indicates that the ovary is subject to inflammaging, a state of chronic low-grade inflammation (Franceschi et al. 2017). Recently, Foley et al. (2021) postulated that MNGCs are “hallmarks of the aging ovary”.

5.6 The transcriptomic landscape of the CL indicates inflammaging and potentially genomic instability in old mice

Our GO enrichment analysis found immune processes to be over-represented, and cell proliferation processes to be under-represented, in old mice. This mirrors the murine ovarian gene expression data of Zhang et al. (2020), who identified two distinct gene clusters that were changing in the ovary with age. One cluster was enriched in terms related to chromosomal organization, DNA damage repair and -replication, negatively enriched in immune response genes and decreased with age, the other cluster was enriched in terms associated with immune response and increased with age. This may point to a decrease in genomic stability, a hallmark of aging (López-Otín et al. 2013, López-Gil et al. 2023). However, DNA damage repair markers like *Ogg1*, *H2ax* and *Trp53bp1* do not show age-related expression differences in our sample (Kuo & Yang 2008, Loft et al. 2008, Minocherhomji et al. 2020). Still, the dysregulation of two of the proliferation processes under-represented in our old mice, DNA replication and mitosis checkpoints, is a major driver of genomic instability (Aguilera & Gómez-González 2008). The immune processes over-represented in our old mice are immune response upregulation and immune cell differentiation. Five of the twenty genes with the strongest expression increase with age in our CL transcriptomes are inflammatory markers. *Kng1*, *Camk2* and *Zcchc12* are pro-inflammatory markers, *Lrrc33* regulates

the inflammatory response, and *Fcna* mediates the inflammatory response (Tab. 3) (Langhauser et al. 2012, Janowski & Sutterwala 2014, Köhler et al. 2020, Zhu et al. 2020, Cheng et al. 2021, Wang Q. et al. 2021, Wang Y. et al. 2021). This indicates inflammaging in the old mice (Franceschi et al. 2017, 2018). Interestingly, inflammaging and genomic instability are mutually reinforcing (Baechle et al. 2023). Genomic instability induces inflammation directly via leakage of DNA fragments into the cytoplasm, and indirectly via mitochondrial dysfunction leading to cytokine production (Wiley et al. 2016, Erdal et al. 2017). In turn, inflammation leads to formation of reactive oxygen species, causing DNA damage (Dizdaroglu & Jaruga 2012, Blaser et al. 2016).

In pregnancy, anti-inflammation is one of the most important functions of P4 (DeMayo et al. 2002, Schumacher et al. 2014, Li et al. 2016). In pathogen-induced chronic inflammation, P4 suppresses uterine contraction (Teraoka et al. 2022). P4 has also been shown to prevent inflammation-induced preterm labour by preventing expression of inflammatory cytokines and pro-labor factors like *Oxtr* (Herbert et al. 2019). Thus, we speculate that in a state of chronic inflammation, the antagonistic effects of P4 on labour induction can both delay labour induction and diminish uterine contractility. Moreover, the labour-preventing actions of P4 may be amplified if the organ that harbours the P4 production gland is subject to inflammaging. In late pregnancy, age-related chronic inflammation may cause dysregulation of P4, leading to a delay in P4 withdrawal due to P4's inhibitory effect on luteolysis.

6 Conclusion & Outlook

In our line, there are no clear morphological signs of luteolysis or of systemic P4 withdrawal at 17.5 dpc, independent of maternal age. At both 15.5 dpc and 17.5 dpc, the CL of late murine pregnancy shows signs of widespread autophagy, a potential sign for a luteolysis-primed CL. The transcriptomic landscape of the CL of late pregnancy indicates that parturition timing varies individually, as gene expression levels of many luteolysis-related genes differ in one 17.5 dpc individual compared to the other individuals from the same cohort. In particular, P4 catabolism, one of the PGF2α signaling target processes in luteolysis, is more active in this individual, while the other targets, luteal apoptosis and P4 synthesis, are unaltered. Some CL of the same individual contain centrally located, eosinophil clumps of cells, likely erythrocytes. The nature and function of this cell aggregation is unknown, but it possible that the co-occurrence of this morphological anomaly and the difference in luteolysis gene expression are connected.

Because P4 levels are neither different between ages nor between pregnancy time points, we assume that systemic P4 withdrawal is not apparent in our line at 17.5 dpc. Accordingly, the ovarian PGF2α levels, which are not different between ages or pregnancy time points, are very low in all samples. We found accumulations of hemosiderin-laden MNGCs in the ovarian medullae of old mice. MNGCs are only found in aging ovaries and may indicate inflammaging. In line with this, our DGE analysis of CL transcriptomes revealed age-related upregulation of several inflammatory markers (*Kng1*, *Camk2*, *Zcchc12*, *Lrrc33* and *Fcna*), and GO enrichment analysis of CL transcriptomes found an over-representation of immune processes in old mice. The

hemosiderin accumulations in the MNGCs may be signs iron overload, which can lead to DNA damage. GO analysis also found negative enrichment of DNA replication and mitosis checkpoint signaling genes, which drive genomic instability, in old CL transcriptomes. Thus, we argue that the late pregnant ovary of 8-month old mice is affected by inflammaging and genomic instability, two hallmarks of aging. Indeed, inflammaging may lead to P4 dysregulation, potentially affecting uterine contractility and causing dystocia in old mice.

The present data on individual timing of murine luteolysis pathways and age-related ovarian inflammation and genomic instability is exploratory and warrants follow-up investigation. We suggest a thorough histological comparison of 3-month old and 8-month old murine ovaries at 14 dpc and from 17 - 19 dpc in 12-hour-steps using H&E, Perl's and Picosirius Red, a more sensitive method for detection of fibrosis (Briley et al. 2016). To validate our preliminary results, we also suggest checking the same ovaries for 20aHSD and 3BHSD presence, as well as the luteal apoptotic markers CASP8 and CASP3, the inflammatory marker CAMK2, and the proliferation marker KI67, by way of immunohistochemistry, accompanied by serum P4 measurements. This way, one can hope to acquire a comprehensive picture of structural luteolysis, and the relative timing of PGF2α signaling-induced P4 catabolism and P4 synthesis inhibition.

7 Sources

Aguilera, A., & Gómez-González, B. (2008). Genome instability: a mechanistic view of its causes and consequences. Nature Reviews Genetics, 9(3), 204-217.

Anders, S., & Huber, W. (2010). Differential expression analysis for sequence count data. Genome biology, 11(10), R106. https://doi.org/10.1186/gb-2010-11-10-r106

Andrews S. (2010). FastQC: a quality control tool for high throughput sequence data. Available online at: http://www.bioinformatics.babraham.ac.uk/projects/fastqc

Archbald, L. F., Al-Bagdadi, F., & Godke, R. A. (1981). A light and electron microscopic study of the periparturient bovine corpus luteum. Theriogenology, 16(1), 27–37. https://doi.org/10.1016/0093-691x(81)90110-2

Asano Y. (2012). Age-related accumulation of non-heme ferric and ferrous iron in mouse ovarian stroma visualized by sensitive non-heme iron histochemistry. The journal of histochemistry and cytochemistry : official journal of the Histochemistry Society, 60(3), 229–242. https://doi.org/10.1369/0022155411431734

Auletta, F. J., & Flint, A. P. (1988). Mechanisms controlling corpus luteum function in sheep, cows, nonhuman primates, and women especially in relation to the time of luteolysis. Endocrine Reviews, 9(1), 88-105.

Baars, J. (2012). Aging and the Art of Living. JHU Press.

Baechle, J. J., Chen, N., Makhijani, P., Winer, S., Furman, D., & Winer, D. A. (2023). Chronic inflammation and the hallmarks of aging. Molecular metabolism, 74, 101755. https://doi.org/10.1016/j.molmet.2023.101755

Bao, Y., Yao, X., Li, X., Ei-Samahy, M. A., Yang, H., Liang, Y., ... & Wang, F. (2021). INHBA transfection regulates proliferation, apoptosis and hormone synthesis in sheep granulosa cells. Theriogenology, 175, 111-122.

Benjamini, Y., & Hochberg, Y. (1995). Controlling the false discovery rate: a practical and powerful approach to multiple testing. Journal of the Royal statistical society: series B (Methodological), 57(1), 289-300.

Blaser, H., Dostert, C., Mak, T. W., & Brenner, D. (2016). TNF and ROS Crosstalk in Inflammation. Trends in cell biology, 26(4), 249–261. https://doi.org/10.1016/j.tcb.2015.12.002

Bremer, A. A., Miller W. L. (2014) Chapter 13 - Regulation of Steroidogenesis. In U. Alfredo & P. M. Conn (Eds.) Cellular Endocrinology in Health and Disease (1st ed., pp. 207-227). Associated Press. https://doi.org/10.1016/B978-0-12-408134-5.00013-5.

Byers, S. L., Wiles, M. V., Dunn, S. L., & Taft, R. A. (2012). Mouse estrous cycle identification tool and images. PloS one, 7(4), e35538. https://doi.org/10.1371/journal.pone.0035538

Camaioni, A., Ucci, M. A., Campagnolo, L., De Felici, M., Klinger, F. G., & Italian Society of Embryology, Reproduction and Research (SIERR) (2022). The process of ovarian aging: it is not just about oocytes and granulosa cells. Journal of assisted

reproduction and genetics, 39(4), 783–792. https://doi.org/10.1007/s10815-022-02478-0

Cheng, X., Liu, D., Song, H., Tian, X., Yan, C., & Han, Y. (2021). Overexpression of Kininogen-1 aggravates oxidative stress and mitochondrial dysfunction in DOX-induced cardiotoxicity. Biochemical and biophysical research communications, 550, 142–150. https://doi.org/10.1016/j.bbrc.2021.02.104

Choi, J., Jo, M., Lee, E., & Choi, D. (2011). The role of autophagy in corpus luteum regression in the rat. Biology of reproduction, 85(3), 465–472. https://doi.org/10.1095/biolreprod.111.091314

Clark, B. J., & Stocco, D. M. (2014). The steroidogenic acute regulatory protein (StAR). Cholesterol Transporters of the START Domain Protein Family in Health and Disease: START Proteins-Structure and Function, 15-47.

Cohn, A. E., & Lange, F. (1930). Studies on the blood vessels in the membranes of chick embryos: Part III. Anatomy and physiology of the blood vessels at different ages. The Journal of experimental medicine, 52(1), 81–87. https://doi.org/10.1084/jem.52.1.81

Davis, J. S., & Rueda, B. R. (2002). The corpus luteum: an ovarian structure with maternal instincts and suicidal tendencies. Frontiers in Bioscience-Landmark, 7(4), 1949-1978.

Deanesly, R. (1930). The corpora lutea of the mouse, with special reference to fat accumulation during the oestrous cycle. Proceedings of the Royal Society of London. Series B, Containing Papers of a Biological Character, 106(747), 578-595.

DeMayo, F. J., Zhao, B., Takamoto, N., & Tsai, S. Y. (2002). Mechanisms of action of estrogen and progesterone. Annals of the New York Academy of Sciences, 955, 48–406. https://doi.org/10.1111/j.1749-6632.2002.tb02765.x

Dizdaroglu, M., & Jaruga, P. (2012). Mechanisms of free radical-induced damage to DNA. Free radical research, 46(4), 382–419. https://doi.org/10.3109/10715762.2011.653969

Dobin, A., Davis, C. A., Schlesinger, F., Drenkow, J., Zaleski, C., Jha, S., Batut, P., Chaisson, M., & Gingeras, T. R. (2013). STAR: ultrafast universal RNA-seq aligner. Bioinformatics (Oxford, England), 29(1), 15–21. https://doi.org/10.1093/bioinformatics/bts635

Dos Santos, L., Bertoli, S. R., Ávila, R. A., & Marques, V. B. (2022). Iron overload, oxidative stress and vascular dysfunction: Evidences from clinical studies and animal models. Biochimica et biophysica acta. General subjects, 1866(9), 130172. https://doi.org/10.1016/j.bbagen.2022.130172

Dumont, M., Luu-The, V., Dupont, E., Pelletier, G., & Labrie, F. (1992). Characterization, expression, and immunohistochemical localization of 3 beta-hydroxysteroid dehydrogenase/delta 5-delta 4 isomerase in human skin. The Journal of investigative dermatology, 99(4), 415–421. https://doi.org/10.1111/1523-1747.ep12616131

Edey, L. F., Georgiou, H., O'Dea, K. P., Mesiano, S., Herbert, B. R., Lei, K., ... & Johnson, M. R. (2018). Progesterone, the maternal immune system and the onset of parturition in the mouse. Biology of reproduction, 98(3), 376-395.

Erdal, E., Haider, S., Rehwinkel, J., Harris, A. L., & McHugh, P. J. (2017). A prosurvival DNA damage-induced cytoplasmic interferon response is mediated by end resection factors and is limited by Trex1. Genes & development, 31(4), 353–369. https://doi.org/10.1101/gad.289769.116

Fang, X., Wong, S., & Mitchell, B. F. (1997). Effects of RU486 on estrogen, progesterone, oxytocin, and their receptors in the rat uterus during late gestation. Endocrinology, 138(7), 2763–2768. https://doi.org/10.1210/endo.138.7.5247

Flurkey, K., Currer, J. M., & Harrison, D. E. (2007). Mouse models in aging research. In The mouse in biomedical research (pp. 637-672). Academic Press.

Foley, K. G., Pritchard, M. T., & Duncan, F. E. (2021). Macrophage-derived multinucleated giant cells: hallmarks of the aging ovary. Reproduction (Cambridge, England), 161(2), V5–V9. https://doi.org/10.1530/REP-20-0489

Fortun, J., Verrier, J. D., Go, J. C., Madorsky, I., Dunn, W. A., & Notterpek, L. (2007). The formation of peripheral myelin protein 22 aggregates is hindered by the enhancement of autophagy and expression of cytoplasmic chaperones. Neurobiology of disease, 25(2), 252–265. https://doi.org/10.1016/j.nbd.2006.09.018

Franceschi C. (1989). Cell proliferation, cell death and aging. Aging (Milan, Italy), 1(1), 3–15. https://doi.org/10.1007/BF03323871

Franceschi, C., Garagnani, P., Vitale, G., Capri, M., & Salvioli, S. (2017). Inflammaging and 'Garb-aging'. Trends in Endocrinology & Metabolism, 28(3), 199-212.

Franceschi, C., Garagnani, P., Parini, P., Giuliani, C., & Santoro, A. (2018). Inflammaging: a new immune–metabolic viewpoint for age-related diseases. Nature Reviews Endocrinology, 14(10), 576-590.

Fraser, H. M., Lunn, S. F., Harrison, D. J., & Kerr, J. B. (1999). Luteal regression in the primate: different forms of cell death during naturaland gonadotropin-releasing hormone antagonist or prostaglandin analogue-induced luteolysis. Biology of reproduction, 61(6), 1468–1479. https://doi.org/10.1095/biolreprod61.6.1468

Fuchs, A. R., Fields, M. J., Freidman, S., Shemesh, M., & Ivell, R. (1995). Oxytocin and the timing of parturition. Influence of oxytocin receptor gene expression, oxytocin secretion, and oxytocin-induced prostaglandin F2 alpha and E2 release. Advances in experimental medicine and biology, 395, 405–420.

Galaris, D., Barbouti, A., & Pantopoulos, K. (2019). Iron homeostasis and oxidative stress: An intimate relationship. Biochimica et Biophysica Acta (BBA)-Molecular Cell Research, 1866(12), 118535.

Girsh, E., & Dekel, N. (2002). Involvement of endothelin-1 and its receptors in PGF2αlpha-induced luteolysis in the rat. Molecular reproduction and development, 63(1), 71–78. https://doi.org/10.1002/mrd.10159

Greenwald, G. S. (1986). Hormonal changes associated with estrogen induced luteolysis in the pregnant hamster: a reevaluation of the luteotropic complex. Proceedings of the Society for Experimental Biology and Medicine, 181(2), 284-288.

Gullstrand, B., Mårtensson, U., Sturfelt, G., Bengtsson, A. A., & Truedsson, L. (2009). Complement classical pathway components are all important in clearance of apoptotic and secondary necrotic cells. Clinical and experimental immunology, 156(2), 303–311. https://doi.org/10.1111/j.1365-2249.2009.03896.x

Hansel, W., & Convey, E. M. (1983). Physiology of the estrous cycle. Journal of animal science, 57(suppl_2), 404-424.

Hasumoto, K., Sugimoto, Y., Yamasaki, A., Morimoto, K., Kakizuka, A., Negishi, M., & Ichikawa, A. (1997). Association of expression of mRNA encoding the PGF2α receptor with luteal cell apoptosis in ovaries of pseudopregnant mice. Reproduction, 109(1), 45-51.

Helming, L., & Gordon, S. (2009). Molecular mediators of macrophage fusion. Trends in cell biology, 19(10), 514–522. https://doi.org/10.1016/j.tcb.2009.07.005

Herbert, B. R., Markovic, D., Georgiou, E., Lai, P. F., Singh, N., Yulia, A., & Johnson, M. R. (2019). Aminophylline and progesterone prevent inflammation-induced preterm parturition in the mouse†. Biology of reproduction, 101(4), 813–822. https://doi.org/10.1093/biolre/ioz112

Horvath, S., Garagnani, P., Bacalini, M. G., Pirazzini, C., Salvioli, S., Gentilini, D., Di Blasio, A. M., Giuliani, C., Tung, S., Vinters, H. V., & Franceschi, C. (2015). Accelerated epigenetic aging in Down syndrome. Aging cell, 14(3), 491–495. https://doi.org/10.1111/acel.12325

Iancu, T. C., Deugnier, Y., Halliday, J. W., Powell, L. W., & Brissot, P. (1997). Ultrastructural sequences during liver iron overload in genetic hemochromatosis. Journal of hepatology, 27(4), 628-638.

Isola, J. V. V., Ocañas, S. R., Hubbart, C. R., Ko, S., Mondal, S. A., Hense, J. D., Carter, H. N. C., Schneider, A., Kovats, S., Alberola-Ila, J., Freeman, W. M., & Stout, M. B. (2023). A single-cell atlas of the aging murine ovary. bioRxiv : the preprint server for biology, 2023.04.29.538828. https://doi.org/10.1101/2023.04.29.538828

Janowski, A. M., & Sutterwala, F. S. (2014). Editorial: dialing down inflammation: LRRC33 regulates Toll-like receptor signaling. Journal of leukocyte biology, 96(1), 4–6. https://doi.org/10.1189/jlb.3CE0214-119R

Kadam, A. L., Moodbidri, S. B., & Nandedkar, T. D. (1984). Inhibition of 3 beta-hydroxysteroid dehydrogenase (3 beta-HSD) activity in the granulosa cells of mouse ovarian follicles by follicular fluid peptide. Steroids, 44(6), 497–509. https://doi.org/10.1016/s0039-128x(84)80031-8

Kaeberlein, M., & Tyler, J. K. (2021). A new era for research into aging. eLife, 10, e65286. https://doi.org/10.7554/eLife.65286

Kapfhamer, J., Waite, C., & Ascoli, M. (2018). The Gαq/11-provoked induction of Akr1c18 in murine luteal cells is mediated by phospholipase C. Molecular and cellular endocrinology, 470, 179–187. https://doi.org/10.1016/j.mce.2017.10.012

Kennedy, B. K., Berger, S. L., Brunet, A., Campisi, J., Cuervo, A. M., Epel, E. S., Franceschi, C., Lithgow, G. J., Morimoto, R. I., Pessin, J. E., Rando, T. A., Richardson, A., Schadt, E. E., Wyss-Coray, T., & Sierra, F. (2014). Geroscience: linking aging to chronic disease. Cell, 159(4), 709–713. https://doi.org/10.1016/j.cell.2014.10.039

Köhler, J., Maletzki, C., Koczan, D., Frank, M., Springer, A., Steffen, C., Revenko, A. S., MacLeod, A. R., Mikkat, S., Kreikemeyer, B., & Oehmcke-Hecht, S. (2020). Kininogen supports inflammation and bacterial spreading during Streptococccus Pyogenes Sepsis. EBioMedicine, 58, 102908. https://doi.org/10.1016/j.ebiom.2020.102908

Koering, M. J., & Kirton, K. T. (1973). The effects of prostaglandin F2 alpha on the structure and function of the rabbit ovary. Biology of reproduction, 9(3), 226–245. https://doi.org/10.1093/biolreprod/9.3.226

Kordowitzki, P., Haghani, A., Zoller, J. A., Li, C. Z., Raj, K., Spangler, M. L., & Horvath, S. (2021). Epigenetic clock and methylation study of oocytes from a bovine model of reproductive aging. Aging cell, 20(5), e13349. https://doi.org/10.1111/acel.13349

Kuo, L. J., & Yang, L. X. (2008). Gamma-H2AX - a novel biomarker for DNA double-strand breaks. In vivo (Athens, Greece), 22(3), 305–309.

Lancu, T. C. (1990). Biological and ultrastructural aspects of iron overload: an overview. Pediatric Pathology, 10(1-2), 281-296.

Langhauser, F., Göb, E., Kraft, P., Geis, C., Schmitt, J., Brede, M., Göbel, K., Helluy, X., Pham, M., Bendszus, M., Jakob, P., Stoll, G., Meuth, S. G., Nieswandt, B., McCrae, K. R., & Kleinschnitz, C. (2012). Kininogen deficiency protects from ischemic neurodegeneration in mice by reducing thrombosis, blood-brain barrier damage, and inflammation. Blood, 120(19), 4082–4092. https://doi.org/10.1182/blood-2012-06-440057

Larsen, B. & Hwang, J. (2011). Progesterone interactions with the cervix: translational implications for term and preterm birth. Infectious diseases in obstetrics and gynecology, 2011, 353297. https://doi.org/10.1155/2011/353297

Li, Y., Adur, M. K., Kannan, A., Davila, J., Zhao, Y., Nowak, R. A., Bagchi, M. K., Bagchi, I. C., & Li, Q. (2016). Progesterone Alleviates Endometriosis via Inhibition of Uterine Cell Proliferation, Inflammation and Angiogenesis in an Immunocompetent Mouse Model. PloS one, 11(10), e0165347. https://doi.org/10.1371/journal.pone.0165347

Liu, Q., Merkler, K. A., Zhang, X., & McLean, M. P. (2007). Prostaglandin F2alpha suppresses rat steroidogenic acute regulatory protein expression via induction of Yin

Yang 1 protein and recruitment of histone deacetylase 1
protein. Endocrinology, 148(11), 5209–5219. https://doi.org/10.1210/en.2007-0326

Loft, S., Høgh Danielsen, P., Mikkelsen, L., Risom, L., Forchhammer, L., & Møller, P. (2008). Biomarkers of oxidative damage to DNA and repair.

López-Gil, L., Pascual-Ahuir, A., & Proft, M. (2023). Genomic Instability and Epigenetic Changes during Aging. International journal of molecular sciences, 24(18), 14279. https://doi.org/10.3390/ijms241814279

López-Otín, C., Blasco, M. A., Partridge, L., Serrano, M., & Kroemer, G. (2023). Hallmarks of aging: An expanding universe. Cell, 186(2), 243–278. https://doi.org/10.1016/j.cell.2022.11.001

Love, M. I., Huber, W., & Anders, S. (2014). Moderated estimation of fold change and dispersion for RNA-seq data with DESeq2. Genome biology, 15(12), 550. https://doi.org/10.1186/s13059-014-0550-8

Lye, SJ., Nicholson, B. J., Mascarenhas, M., MacKenzie, L., & Petrocelli, T. (1993). Increased expression of connexin-43 in the rat myometrium during labor is associated with an increase in the plasma estrogen:progesterone ratio. Endocrinology, 132(6), 2380–2386. https://doi.org/10.1210/endo.132.6.8389279

Malven P. V.; Francis R. P. (1969). Structural luteolysis of induced corpora lutea in “androgen-sterilized” rats. , 165(1), 55–60. doi:10.1002/ar.1091650106

McLean, M P; Billheimer, J T; Warden, K J; Irby, R B (1995). Prostaglandin F2 alpha mediates ovarian sterol carrier protein-2 expression during luteolysis.. Endocrinology, 136(11), 4963–4972. doi:10.1210/endo.136.11.7588230

McNally, A. K., & Anderson, J. M. (2005). Multinucleated giant cell formation exhibits features of phagocytosis with participation of the endoplasmic reticulum. Experimental and molecular pathology, 79(2), 126–135. https://doi.org/10.1016/j.yexmp.2005.06.008

McNally, A. K., & Anderson, J. M. (2011). Macrophage fusion and multinucleated giant cells of inflammation. Advances in experimental medicine and biology, 713, 97–111. https://doi.org/10.1007/978-94-007-0763-4_7

Mejia, R., Waite, C., & Ascoli, M. (2015). Activation of Gq/11 in the mouse corpus luteum is required for parturition. Molecular endocrinology (Baltimore, Md.), 29(2), 238–246. https://doi.org/10.1210/me.2014-1324

Milde, R., Ritter, J., Tennent, G. A., Loesch, A., Martinez, F. O., Gordon, S., Pepys, M. B., Verschoor, A., & Helming, L. (2015). Multinucleated Giant Cells Are Specialized for Complement-Mediated Phagocytosis and Large Target Destruction. Cell reports, 13(9), 1937–1948. https://doi.org/10.1016/j.celrep.2015.10.065

Miller, M. A., & Zachary, J. F. (2017). Mechanisms and Morphology of Cellular Injury, Adaptation, and Death. Pathologic Basis of Veterinary Disease, 2–43.e19. https://doi.org/10.1016/B978-0-323-35775-3.00001-1

Milvae, R. A. (2000). Inter-relationships between endothelin and prostaglandin F2alpha in corpus luteum function. Reviews of Reproduction, 5(1), 1-5.

Minocherhomji, S., Liu, Y., He, Y. D., & Fielden, M. R. (2020). Biomarkers of genome instability in normal mammalian genomes following drug-induced replication stress. Environmental and molecular mutagenesis, 61(8), 770–785. https://doi.org/10.1002/em.22364

Miyazaki, E., Kato, J., Kobune, M., Okumura, K., Sasaki, K., Shintani, N., Arosio, P., & Niitsu, Y. (2002). Denatured H-ferritin subunit is a major constituent of haemosiderin in the liver of patients with iron overload. Gut, 50(3), 413–419. https://doi.org/10.1136/gut.50.3.413

Montenegro, L., Magalhães, P., Guerreiro, A. C., Brandão, C., Pinto, A., Almeida, H., Martins-Bessa, A., & Silva, E. (2023). The Contribution of the Sheep and the Goat Model to the Study of Ovarian Ageing. Biology, 12(2), 270. https://doi.org/10.3390/biology12020270

Moriuchi, H., Koda, N., Okuda-Ashitaka, E., Daiyasu, H., Ogasawara, K., Toh, H., Ito, S., Woodward, D. F., & Watanabe, K. (2008). Molecular characterization of a novel type of prostamide/prostaglandin F synthase, belonging to the thioredoxin-like superfamily. The Journal of biological chemistry, 283(2), 792–801. https://doi.org/10.1074/jbc.M705638200

Murr, S. M., Stabenfeldt, G. H., Bradford, G. E., & Geschwind, I. I. (1974). Plasma progesterone during pregnancy in the mouse. Endocrinology, 94(4), 1209–1211. https://doi.org/10.1210/endo-94-4-1209

Nadeem, L., Balendran, R., Dorogin, A., Mesiano, S., Shynlova, O., & Lye, S. J. (2021). Pro-inflammatory signals induce 20α-HSD expression in myometrial cells: A key mechanism for local progesterone withdrawal. Journal of cellular and molecular medicine, 25(14), 6773–6785. https://doi.org/10.1111/jcmm.16681

Nie, C., Li, Y., Li, R., Yan, Y., Zhang, D., Li, T., ... & Xu, X. (2022). Distinct biological ages of organs and systems identified from a multi-omics study. Cell reports, 38(10).

Okita, R. T., & Okita, J. R. (1996). Prostaglandin-metabolizing enzymes during pregnancy: characterization of NAD(+)-dependent prostaglandin dehydrogenase, carbonyl reductase, and cytochrome P450-dependent prostaglandin omega-hydroxylase. Critical reviews in biochemistry and molecular biology, 31(2), 101–126. https://doi.org/10.3109/10409239609106581

Ou, CW., Orsino, A., & Lye, S. J. (1997). Expression of connexin-43 and connexin-26 in the rat myometrium during pregnancy and labor is differentially regulated by mechanical and hormonal signals. Endocrinology, 138(12), 5398–5407. https://doi.org/10.1210/endo.138.12.5624

Ou, CW., Chen, ZQ., Qi S. & Lye, SJ. (1998). Increased expression of the rat myometrial oxytocin receptor messenger ribonucleic acid during labor requires both mechanical and hormonal signals. Biology of reproduction, 59(5), 1055–1061. https://doi.org/10.1095/biolreprod59.5.1055

Park, J. Y., Jang, H., Curry, T. E., Sakamoto, A., & Jo, M. (2013). Prostate androgen-regulated mucin-like protein 1: a novel regulator of progesterone

metabolism. Molecular endocrinology (Baltimore, Md.), 27(11), 1871–1886. https://doi.org/10.1210/me.2013-1097

Paavola L. G. (1979). The corpus luteum of the guinea pig. IV. Fine structure of macrophages during pregnancy and postpartum luteolysis, and the phagocytosis of luteal cells. The American journal of anatomy, 154(3), 337–364. https://doi.org/10.1002/aja.1001540304

Piekorz, R. P., Gingras, S., Hoffmeyer, A., Ihle, J. N., & Weinstein, Y. (2005). Regulation of progesterone levels during pregnancy and parturition by signal transducer and activator of transcription 5 and 20alpha-hydroxysteroid dehydrogenase. Molecular endocrinology (Baltimore, Md.), 19(2), 431–440. https://doi.org/10.1210/me.2004-0302

Recalcati, S., & Cairo, G. (2021). Macrophages and Iron: A Special Relationship. Biomedicines, 9(11), 1585. https://doi.org/10.3390/biomedicines9111585

Reid, D., Snell, G., Ward, C., Krishnaswamy, R., Ward, R., Zheng, L. , ... & Walters, H. (2001). Iron overload and nitric oxide-derived oxidative stress following lung transplantation. The Journal of heart and lung transplantation, 20(8), 840-849.

Roizen, J. D., Asada, M., Tong, M., Tai, H. H., & Muglia, L. J. (2008). Preterm birth without progesterone withdrawal in 15-hydroxyprostaglandin dehydrogenase hypomorphic mice. Molecular endocrinology (Baltimore, Md.), 22(1), 105–112. https://doi.org/10.1210/me.2007-0178

Roizen, J. D., Asada, M., Tong, M., Tai, H. H., & Muglia, L. J. (2019). Early pregnancy loss in 15-hydroxyprostaglandin dehydrogenase knockout (15-HPGD-/-) mice due to requirement for embryo 15-HPGD activity. Scientific reports, 9(1), 17612. https://doi.org/10.1038/s41598-019-54064-7

Rubin B. S. (2000). Hypothalamic alterations and reproductive aging in female rats: evidence of altered luteinizing hormone-releasing hormone neuronal function. Biology of reproduction, 63(4), 968–976. https://doi.org/10.1095/biolreprod63.4.968

Ryter, S. W., Cloonan, S. M., & Choi, A. M. (2013). Autophagy: a critical regulator of cellular metabolism and homeostasis. Molecules and cells, 36, 7-16.

Sakamoto, K., Miwa, K., Ezashi, T., Okuda-Ashitaka, E., Okuda, K., Houtani, T., ... & Hayaishi, O. (1995). Expression of mRNA encoding the prostaglandin F2α receptor in bovine corpora lutea throughout the oestrous cycle and pregnancy. Reproduction, 103(1), 99-105.

Sato J, Hashimoto S, Doi T, Yamada N, Tsuchitani M. Histological characteristics of the regression of corpora lutea in wistar hannover rats: the comparisons with sprague-dawley rats. J Toxicol Pathol. 2014 Jul;27(2):107-13. doi: 10.1293/tox.2013-0054. Epub 2014 Feb 24. PMID: 25352711; PMCID: PMC4110934.

Schumacher, A., Costa, S. D., & Zenclussen, A. C. (2014). Endocrine factors modulating immune responses in pregnancy. Frontiers in immunology, 5, 196. https://doi.org/10.3389/fimmu.2014.00196

Singh, G., Singh, M. M., Maitra, S. C., Elger, W., Kalra, V., Upadhyay, S. N., Chowdhury, S. R., & Kamboj, V. P. (1988). Luteolytic action of two antiprogestational agents (RU-38486 and ZK-98734) in the rat. Journal of reproduction and fertility, 83(1), 73–83. https://doi.org/10.1530/jrf.0.0830073

Sirard M. A. (2022). Why is the human ovary aging faster than other organs?. Women & health, 62(7), 577–579. https://doi.org/10.1080/03630242.2022.2105776

Stocco, C. O., Zhong, L., Sugimoto, Y., Ichikawa, A., Lau, L. F., & Gibori, G. (2000). Prostaglandin F2alpha-induced expression of 20alpha-hydroxysteroid dehydrogenase involves the transcription factor NUR77. The Journal of biological chemistry, 275(47), 37202–37211. https://doi.org/10.1074/jbc.M006016200

Stocco, C., Callegari, E., & Gibori, G. (2001). Opposite effect of prolactin and prostaglandin F2α on the expression of luteal genes as revealed by rat cDNA expression array. Endocrinology, 142(9), 4158-4161.

Stocco, C. O., Lau, L. F., & Gibori, G. (2002). A calcium/calmodulin-dependent activation of ERK1/2 mediates JunD phosphorylation and induction of nur77 and 20alpha-hsd genes by prostaglandin F2alpha in ovarian cells. The Journal of biological chemistry, 277(5), 3293–3302. https://doi.org/10.1074/jbc.M110936200

Stocco, C., Telleria, C., & Gibori, G. (2007). The molecular control of corpus luteum formation, function, and regression. Endocrine reviews, 28(1), 117-149.

Sugimoto, Y., Segi, E., Tsuboi, K., Ichikawa, A., Narumiya, S. (1998). Female Reproduction in Mice Lacking the Prostaglandin F Receptor. In: Zingg, H.H., Bourque, C.W., Bichet, D.G. (eds) Vasopressin and Oxytocin. Advances in Experimental Medicine and Biology, vol 449. Springer, Boston, MA. https://doi.org/10.1007/978-1-4615-4871-3_39

Sugino, N., Telleria, C. M., & Gibori, G. (1997). Progesterone inhibits 20alpha-hydroxysteroid dehydrogenase expression in the rat corpus luteum through the glucocorticoid receptor. Endocrinology, 138(10), 4497–4500. https://doi.org/10.1210/endo.138.10.5572

Sugino, N., & Okuda, K. (2007). Species-related differences in the mechanism of apoptosis during structural luteolysis. The Journal of reproduction and development, 53(5), 977–986. https://doi.org/10.1262/jrd.19047

Tang, Z., Huang, Y., Zhang, Z., Tang, Y., Chen, J., Sun, F., Yang, H., & Wang, Z. (2017). Accumulated autophagosomes and excessive apoptosis during the luteal development of pregnant rats. International journal of clinical and experimental pathology, 10(12), 11384–11392.

Teraoka, Y., Sugimoto, J., Konishi, H., Miyoshi, H., Furusho, H., Miyauchi, M., Kajioka, S., Koh, I., & Kudo, Y. (2022). Progesterone Suppresses Uterine Contraction by Reducing Odontogenic Porphyromonas gingivalis Induced Chronic Inflammation in Mice. Biomolecules, 12(8), 1029. https://doi.org/10.3390/biom12081029

Urzua, U., Chacon, C., Espinoza, R., Martínez, S., & Hernandez, N. (2018). Parity-Dependent Hemosiderin and Lipofuscin Accumulation in the Reproductively Aged

Mouse Ovary. Analytical cellular pathology (Amsterdam), 2018, 1289103. https://doi.org/10.1155/2018/1289103

Vázquez-Nin, G.H., Escobar, M.L., Echeverría, O.M. (2011). Luteolysis. In: Cell Death in Mammalian Ovary. Springer, Dordrecht. https://doi.org/10.1007/978-94-007-1134-1_14

Wada, Y., Ozaki, H., Abe, N., Mori, A., Sakamoto, K., Nagamitsu, T., Nakahara, T., & Ishii, K. (2013). Role of vascular endothelial growth factor in maintenance of pregnancy in mice. Endocrinology, 154(2), 900–910. https://doi.org/10.1210/en.2012-1967

Waite, C., Mejia, R., & Ascoli, M. (2016). Gq/11-Dependent Changes in the Murine Ovarian Transcriptome at the End of Gestation. Biology of reproduction, 94(3), 62. https://doi.org/10.1095/biolreprod.115.136952

Wald, A. (1943). Tests of statistical hypotheses concerning several parameters when the number of observations is large. Transactions of the American Mathematical society, 54(3), 426-482.

Walton, K. L., Goney, M. P., Peppas, Z., Stringer, J. M., Winship, A., Hutt, K., ... & Harrison, C. A. (2022). Inhibin inactivation in female mice leads to elevated FSH levels, ovarian overstimulation, and pregnancy loss. Endocrinology, 163(4), bqac025.

Wang, Y., Juan, L. V., Ma, X., Wang, D., Ma, H., Chang, Y., Nie, G., Jia, L., Duan, X., & Liang, X. J. (2010). Specific hemosiderin deposition in spleen induced by a low dose of cisplatin: altered iron metabolism and its implication as an acute hemosiderin formation model. Current drug metabolism, 11(6), 507–515. https://doi.org/10.2174/138920010791636149

Wang, Q., Hernández-Ochoa, E. O., Viswanathan, M. C., Blum, I. D., Do, D. C., Granger, J. M., Murphy, K. R., Wei, A. C., Aja, S., Liu, N., Antonescu, C. M., Florea, L. D., Talbot, C. C., Jr, Mohr, D., Wagner, K. R., Regot, S., Lovering, R. M., Gao, P., Bianchet, M. A., Wu, M. N., … Anderson, M. E. (2021). CaMKII oxidation is a critical performance/disease trade-off acquired at the dawn of vertebrate evolution. Nature communications, 12(1), 3175. https://doi.org/10.1038/s41467-021-23549-3

Wang, Y., Yu, Y., Pang, Y., Yu, H., Zhang, W., Zhao, X., & Yu, J. (2021). The distinct roles of zinc finger CCHC-type (ZCCHC) superfamily proteins in the regulation of RNA metabolism. RNA biology, 18(12), 2107-2126.

Wiley, C. D., Velarde, M. C., Lecot, P., Liu, S., Sarnoski, E. A., Freund, A., Shirakawa, K., Lim, H. W., Davis, S. S., Ramanathan, A., Gerencser, A. A., Verdin, E., & Campisi, J. (2016). Mitochondrial Dysfunction Induces Senescence with a Distinct Secretory Phenotype. Cell metabolism, 23(2), 303–314. https://doi.org/10.1016/j.cmet.2015.11.011

Yoshimoto, F. K., Gonzalez, E., Auchus, R. J., & Guengerich, F. P. (2016). Mechanism of 17α,20-Lyase and New Hydroxylation Reactions of Human Cytochrome P450 17A1: 18O labeling and oxygen surrogate evidence for a role of a perferryl oxygen. The Journal of biological chemistry, 291(33), 17143–17164. https://doi.org/10.1074/jbc.M116.732966

Yu, B., Zeng, A., Liu, H., Yang, Z., & Fu, M. (2022). MiR-654-3p, reduced by the excessive ALKBH5, Alleviated the Inflammation in OA by targeting TNFRSF9, the trigger of the NF-κB pathway. Biochemical and biophysical research communications, 634, 30–39. https://doi.org/10.1016/j.bbrc.2022.09.103

Zhang, X., Li, J., Liu, J., Luo, H., Gou, K., & Cui, S. (2013). Prostaglandin F2α upregulates Slit/Robo expression in mouse corpus luteum during luteolysis. The Journal of endocrinology, 218(3), 299–310. https://doi.org/10.1530/JOE-13-0088

Zhang, X., Mi, M., Hao, W., Fan, Q., & Gao, B. (2017). Progesterone down-regulates SLIT/ROBO expression in mouse corpus luteum. Acta histochemica, 119(7), 740–746. https://doi.org/10.1016/j.acthis.2017.09.006

Zhang, Z., Schlamp, F., Huang, L., Clark, H., & Brayboy, L. (2020). Inflammaging is associated with shifted macrophage ontogeny and polarization in the aging mouse ovary. Reproduction (Cambridge, England), 159(3), 325–337. https://doi.org/10.1530/REP-19-0330

Zhu, A., Ibrahim, J. G., & Love, M. I. (2019). Heavy-tailed prior distributions for sequence count data: removing the noise and preserving large differences. Bioinformatics (Oxford, England), 35(12), 2084–2092. https://doi.org/10.1093/bioinformatics/bty895

Zhu, G., Zhao, G., Lin, J., Li, C., Wang, Q., Xu, Q., Peng, X., & Zheng, H. (2020). FCN-A mediates the inflammatory response and the macrophage polarization in Aspergillus fumigatus keratitis of mice by activating the MAPK signaling pathway. International immunopharmacology, 83, 106473. https://doi.org/10.1016/j.intimp.2020.106473